Clinical and Translational Report

Cell Metabolism

Pimozide Alleviates Hyperglycemia in Diet-Induced Obesity by Inhibiting Skeletal Muscle Ketone Oxidation

Graphical Abstract

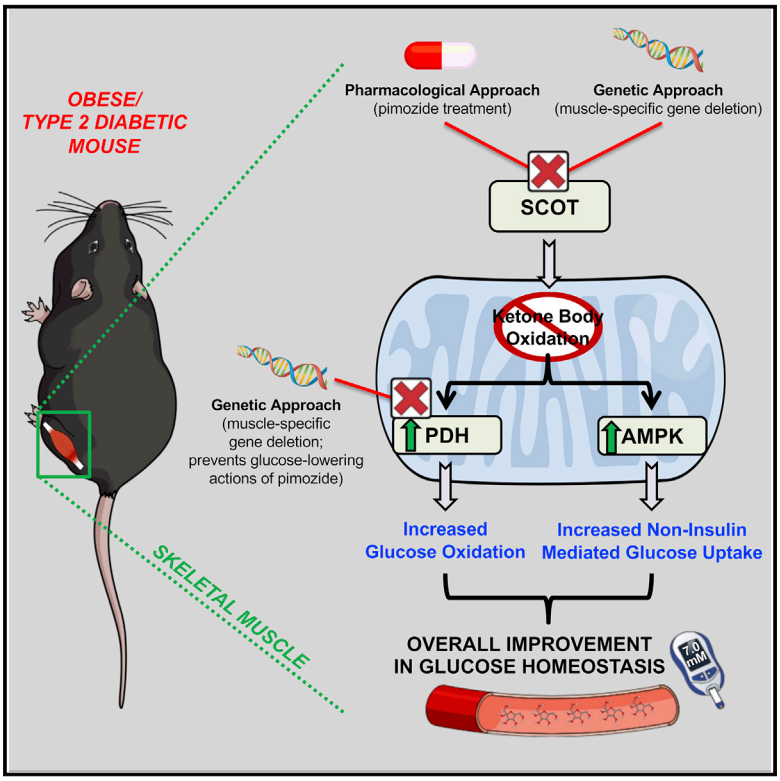

Highlights

- Skeletal muscle SCOT expression and activity are elevated in obesity
- Selective elimination of skeletal muscle SCOT activity improves glycemia in obese mice
- Pimozide is a SCOT antagonist that improves glycemia in obese mice
- SCOT antagonism within skeletal muscle improves glycemia by increasing PDH activity

Authors

Rami Al Batran, Keshav Gopal, Megan E. Capozzi, ..., Jonathan E. Campbell, Jason R.B. Dyck, John R. Ussher

Correspondence

jussher@ualberta.ca

In Brief

Al Batran et al. demonstrate that the rate-limiting enzyme of ketone oxidation, succinyl CoA:3-ketoacid CoA transferase (SCOT), is elevated in skeletal muscles of diet-induced obese mice. This metabolic perturbation is maladaptive, as pharmacological and genetic strategies aimed at reducing skeletal muscle SCOT activity elicited a robust glucose-lowering response in obese mice.

Al Batran et al., 2020, Cell Metabolism *31*, 1–11
May 5, 2020
https://doi.org/10.1016/j.cmet.2020.03.017

CellPress

Please cite this article in press as: Al Batran et al., Pimozide Alleviates Hyperglycemia in Diet-Induced Obesity by Inhibiting Skeletal Muscle Ketone Oxidation, Cell Metabolism (2020), https://doi.org/10.1016/j.cmet.2020.03.017

Cell Metabolism
Clinical and Translational Report

Pimozide Alleviates Hyperglycemia in Diet-Induced Obesity by Inhibiting Skeletal Muscle Ketone Oxidation

Rami Al Batran,[1,2,3,14] Keshav Gopal,[1,2,3] Megan E. Capozzi,[11] Jadin J. Chahade,[1,2,3] Bruno Saleme,[5] S. Amirhossein Tabatabaei-Dakhili,[1] Amanda A. Greenwell,[1,2,3] Jingjing Niu,[11] Malak Almutairi,[1,2,3] Nikole J. Byrne,[2,3,4] Grant Masson,[2,3,4] Ryekjang Kim,[1,2,3] Farah Eaton,[1,2,3] Erin E. Mulvihill,[6,7] Léa Garneau,[6,8] Andrea R. Masters,[12] Zeruesenay Desta,[13] Carlos A. Velázquez-Martínez,[1] Céline Aguer,[6,8,9] Peter A. Crawford,[10] Gopinath Sutendra,[5] Jonathan E. Campbell,[11] Jason R.B. Dyck,[2,3,4] and John R. Ussher[1,2,3,15,*]

[1]Faculty of Pharmacy and Pharmaceutical Sciences, University of Alberta, Edmonton, AB, Canada
[2]Alberta Diabetes Institute, University of Alberta, Edmonton, AB, Canada
[3]Cardiovascular Research Centre, University of Alberta, Edmonton, AB, Canada
[4]Department of Pediatrics, University of Alberta, Edmonton, AB, Canada
[5]Department of Medicine, University of Alberta, Edmonton, AB, Canada
[6]Department of Biochemistry, Microbiology & Immunology, University of Ottawa, Ottawa, ON, Canada
[7]University of Ottawa Heart Institute, Ottawa, ON, Canada
[8]Institut du Savoir Montfort, Ottawa, ON, Canada
[9]School of Human Kinetics, University of Ottawa, Ottawa, ON, Canada
[10]Division of Molecular Medicine, Department of Medicine, Department of Biochemistry, Molecular Biology, and Biophysics, University of Minnesota, Minneapolis, MN, USA
[11]Duke Molecular Physiology Institute, Duke University, Durham, NC, USA
[12]Indiana University School of Medicine, Indiana University Melvin and Bren Simon Cancer Center, Indianapolis, IN, USA
[13]Department of Medicine, Division of Clinical Pharmacology, Indianapolis, IN, USA
[14]Present address: Faculty of Pharmacy, Université de Montréal, Montreal, QC, Canada
[15]Lead Contact
*Correspondence: jussher@ualberta.ca
https://doi.org/10.1016/j.cmet.2020.03.017

SUMMARY

Perturbations in carbohydrate, lipid, and protein metabolism contribute to obesity-induced type 2 diabetes (T2D), though whether alterations in ketone body metabolism influence T2D pathology is unknown. We report here that activity of the rate-limiting enzyme for ketone body oxidation, succinyl-CoA:3-ketoacid-CoA transferase (SCOT/*Oxct1*), is increased in muscles of obese mice. We also found that the diphenylbutylpiperidine pimozide, which is approved to suppress tics in individuals with Tourette syndrome, is a SCOT antagonist. Pimozide treatment reversed obesity-induced hyperglycemia in mice, which was phenocopied in mice with muscle-specific *Oxct1*/SCOT deficiency. These actions were dependent on pyruvate dehydrogenase (PDH/*Pdha1*) activity, the rate-limiting enzyme of glucose oxidation, as pimozide failed to alleviate hyperglycemia in obese mice with a muscle-specific *Pdha1*/PDH deficiency. This work defines a fundamental contribution of enhanced ketone body oxidation to the pathology of obesity-induced T2D, while suggesting pharmacological SCOT inhibition as a new class of anti-diabetes therapy.

INTRODUCTION

Obesity is a significant risk factor for skeletal muscle insulin resistance, which elicits hyperglycemia and is a major predictor for the future development of T2D (DeFronzo et al., 2015;

Context and Significance

While alterations in carbohydrate, fat, and protein metabolism can contribute to obesity-induced type 2 diabetes (T2D), there is limited information on obesity's impact on ketone metabolism, an area of growing interest with increased use of ketogenic diets to combat obesity. Moreover, it remains unknown whether manipulating ketone metabolism influences the pathology of obesity and T2D. Al Batran and colleagues have identified that activity of the ketone oxidation enzyme, succinyl CoA:3-ketoacid CoA transferase (SCOT), is increased in the muscles of obese mice. They have also identified that an antipsychotic drug, pimozide, can block the actions of SCOT, which produces a potent blood sugar lowering effect in obese mice. Therefore, blocking muscle SCOT activity may be a potential therapeutic approach for improving blood sugar control in obesity and T2D.

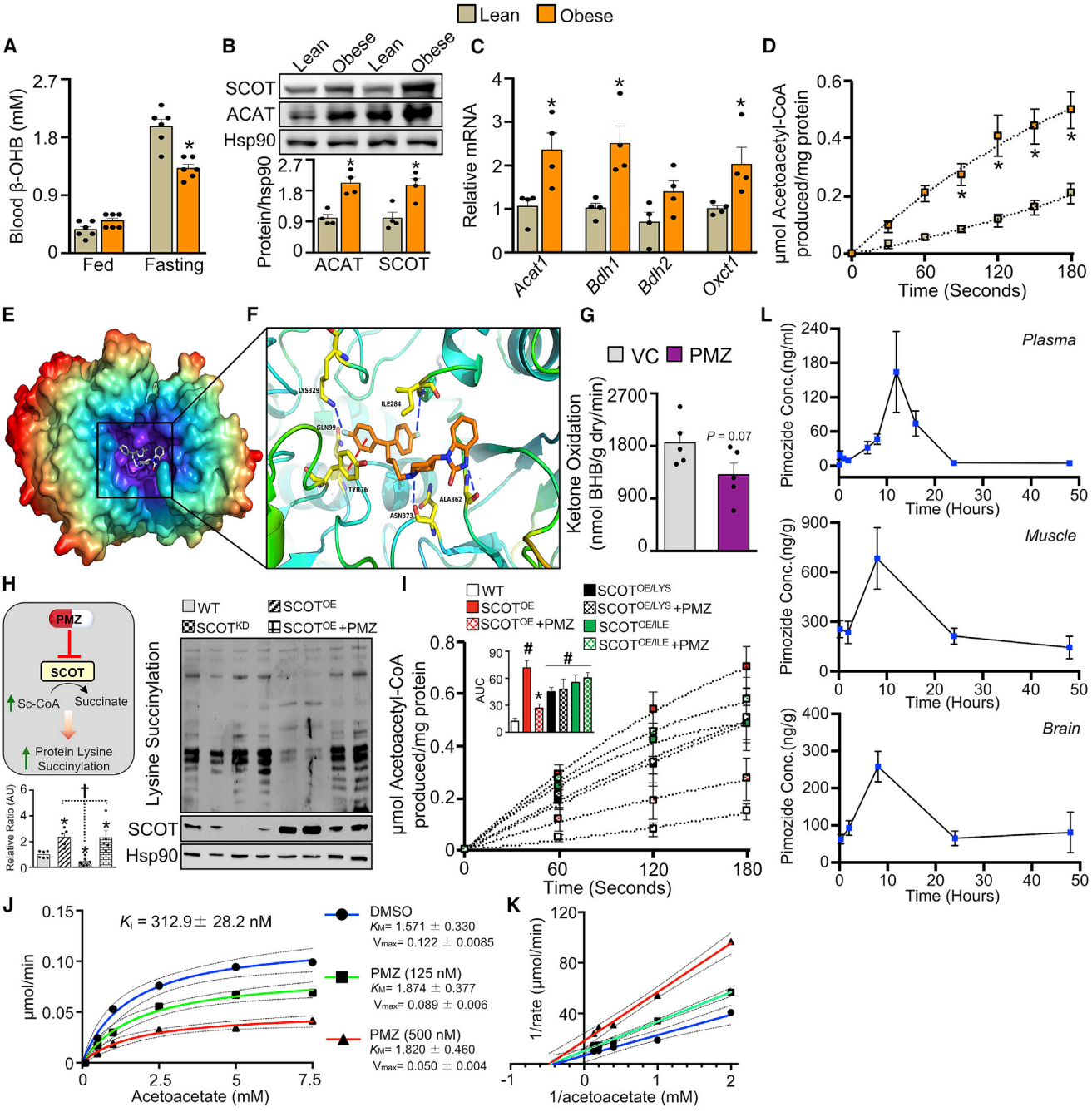

Figure 1. Pimozide Is a Succinyl-CoA:3-Ketoacid CoA Transferase (SCOT) Antagonist

(A) Circulating βOHB levels (n = 6).

(B) SCOT and acetoacetyl CoA thiolase (ACAT1) protein expression normalized to heat shock protein 90 (Hsp90) in mouse gastrocnemius muscles (n = 4–6).

(C) mRNA expression for genes regulating ketone body oxidation in mouse gastrocnemius muscles (n = 4).

(D) SCOT activity in gastrocnemius muscles from lean and obese mice (n = 4 or 5).

(E) Molecular docking of pimozide (PMZ) in the D-oxyanion pocket of SCOT.

(F) Modeling of PMZ within SCOT's D-oxyanion pocket and key amino acid residues PMZ interacts with to theoretically inhibit SCOT catalytic activity. Blue dashed line, hydrogen bond; red dashed line, hydrophobic interaction.

(G) βOHB oxidation rates in C57BL/6J working mouse hearts treated with vehicle control (VC) or PMZ (n = 5).

(H) PMZ-mediated inhibition of SCOT increases succinyl CoA (Sc-CoA) substrate needed for protein succinylation, as depicted by immunoblots for protein lysine succinylation in C2C12 myotubes transfected with the following: wild-type (WT) SCOT, SCOT knockdown ($SCOT^{KD}$), SCOT overexpression ($SCOT^{OE}$), and $SCOT^{OE}$ treated with PMZ (n = 5 or 6). *p < 0.05 versus WT, †p < 0.05 versus $SCOT^{OE}$.

(I) SCOT activity following transfection of C2C12 myotubes with our various SCOT mutants and treated with VC or PMZ (10 µM) (n = 4–6). LYS, lysine-368 mutant; ILE, isoleucine-323 mutant. #p < 0.05 versus WT, *p < 0.05 versus $SCOT^{OE}$.

(legend continued on next page)

Samuel and Shulman, 2012). A plethora of evidence indicates that perturbations in skeletal muscle glucose, fatty acid, and branched-chain amino acid metabolism contribute to the pathology of obesity-induced hyperglycemia (Muoio and Neufer, 2012; Newgard, 2012; Samuel and Shulman, 2012). Conversely, whether perturbations in muscle ketone body oxidation occur during obesity and contribute to obesity-induced impairments in muscle insulin sensitivity and hyperglycemia remains unknown. Ketone bodies (e.g., β-hydroxybutyrate [βOHB] and acetoacetate) are produced in the liver during prolonged fasting, in order to provide the brain with an alternative fuel source to glucose, as the brain has limited capacity to oxidize fatty acids for energy production. This confers a physiological advantage by reducing muscle proteolysis, which provides amino acids for supporting hepatic gluconeogenesis during prolonged fasting (Puchalska and Crawford, 2017; Robinson and Williamson, 1980). However, other oxidative tissues like the heart and skeletal muscle are also capable of oxidizing ketone bodies. Of interest, ketone body utilization rates appear to be enhanced in the skeletal muscle of a small number of obese and diabetic patients (Hall et al., 1984; Vice et al., 2005), and studies have suggested that ketone bodies may be the preferred energy source for oxidative metabolism of resting muscle (Ruderman and Goodman, 1973). Our objective was to characterize the potential perturbations in ketone body metabolism that take place in skeletal muscle in response to experimental obesity as well as to determine whether these changes could be pharmacologically targeted as a means of improving hyperglycemia.

RESULTS AND DISCUSSION

Ketone Body Oxidation Enzyme Expression Is Increased in Skeletal Muscle following Experimental Obesity

C57BL/6J mice subjected to high-fat diet (HFD)-induced obesity (Research Diets D12492 [60% kcal lard], herein referred to as obese mice) exhibited marked reductions in circulating βOHB levels versus their lean counterparts following an overnight fast (Figure 1A). It has been postulated that impaired hepatic ketogenesis is the primary driver of the obesity-mediated decline in fasting βOHB levels (Cotter et al., 2014; d'Avignon et al., 2018). On the contrary, mRNA and/or protein expression of ketone body oxidation enzymes *Oxct1*/SCOT (which will be referred to as SCOT throughout), acetoacetyl CoA thiolase (*Acat1*/ACAT1), and βOHB dehydrogenase (*Bdh1*/*Bdh2*) were all increased in gastrocnemius muscles of obese mice (Figures 1B and 1C). Moreover, gastrocnemius muscle SCOT activity was also increased in obese mice (Figure 1D). Taken together, we posit that the obesity-mediated decline in circulating βOHB levels during fasting is due to a combination of both reduced hepatic ketogenesis as well as an increase in skeletal muscle ketone body utilization.

Pimozide Is a SCOT Antagonist

Whether the increase in skeletal muscle ketone body oxidation is an adaptive or maladaptive response during the progression of obesity-induced hyperglycemia is unclear. Addressing this uncertainty is confounded by the fact that no known pharmacological modulators of ketone body oxidation have been identified and characterized to date. We thus embarked on a virtual high-throughput screening (vHTS) campaign to discover potential antagonists of SCOT, since SCOT is not present in the liver, and thus inhibiting SCOT would not impact hepatic ketogenesis, unlike an ACAT or βOHB dehydrogenase antagonist would. Our vHTS started with 2,924 commercially approved US Food and Drug Administration (FDA) agents from the ZINC database. Pimozide, an FDA-approved agent for controlling tics in individuals with Tourette syndrome (Colvin and Tankanow, 1985), was selected for further study based on its binding energy, binding interaction types, and ligand orientation in the SCOT oxyanion pocket (Figures 1E and 1F). As the heart is the most metabolically demanding organ and an avid consumer of ketones (Lopaschuk and Ussher, 2016; Puchalska and Crawford, 2017), we next perfused isolated working mouse hearts with vehicle control (VC) or pimozide and confirmed that pimozide reduces ketone body oxidation without impacting heart rate or cardiac function (Figures 1G and S1A–S1D). Treatment of C2C12 myotubes with pimozide also increased the accumulation of intracellular [^{13}C]βOHB (55.4 μM [VC] versus 114.9 μM [pimozide]), consistent with an inhibition of SCOT activity. Because SCOT requires succinyl-CoA as a substrate, which is required for protein succinylation (Hirschey and Zhao, 2015), we next knocked down or overexpressed SCOT in C2C12 myotubes via siRNA or plasmid-mediated transfection, respectively, and assessed overall protein lysine succinylation. siRNA knockdown of SCOT augmented lysine succinylation, whereas SCOT overexpression abolished lysine succinylation and was prevented via treatment with pimozide (Figure 1H). Furthermore, our vHTS indicated that pimozide binding within the SCOT oxyanion pocket requires residues Lys^{329} and Ile^{284} (Figures S1E and S1F). Hence, we mutated these two sites and transfected C2C12 myotubes with these new SCOT mutants, both of which abrogated pimozide's ability to inhibit SCOT (Figure 1I), reinforcing the key role these residues exert in mediating pimozide's ability to inhibit SCOT. Last, we performed an *in vitro* enzyme kinetics assessment, which indicated that pimozide is a noncompetitive inhibitor of SCOT (Ki = 312.9 ± 28.2 nM) (Figures 1J and 1K).

Pharmacological SCOT Inhibition Improves Glycemia in Obese Mice

To ascertain whether enhanced muscle SCOT activity is adaptive or maladaptive with relation to obesity-induced hyperglycemia, we subjected C57BL/6J male mice to experimental HFD-induced obesity for 10 weeks. All mice were subsequently randomized to treatment with either VC or pimozide (10 mg/kg once every 2.5 days via oral gavage) for 2 weeks.

(J and K) Michaelis-Menten kinetics (J) and Lineweaver-Burk plot (K) for SCOT inhibition via PMZ (n = 3).

(L) Plasma, gastrocnemius muscle, and brain levels of pimozide at various time points (up to 48 h) following a single oral gavage of pimozide in obese mice (n = 3).

Values represent means ± SEM. Differences were determined by the use of an unpaired two-tailed Student's t test, or one- or two-way ANOVA followed by a Bonferroni post hoc analysis. *p < 0.05 versus control/lean. See also Figure S1.

Pharmacokinetics assessment following oral gavage of pimozide at this dose demonstrates peak circulating concentrations at ~12 h post-gavage, though the drug remains detectable in plasma at clinically relevant levels (~5 ng/mL) and tissue 48 h post-gavage (Figure 1L), a profile differing from that in humans, where peak levels are reached at ~8 h (Sallee et al., 1987). Treatment with pimozide had no impact on random-fed state βOHB levels but increased circulating βOHB levels during an overnight fast, which was associated with a reduction in circulating glucose levels (Figures 2A and 2B). The pimozide-induced increase in fasting βOHB levels was not associated with changes in the mRNA expression of genes regulating hepatic ketogenesis or muscle ketone body utilization (Figure S1G). Interestingly, pimozide treatment enhanced glucose tolerance following an overnight fast (Figure 2C), which was associated with reduced circulating insulin levels (Figure 2D), suggesting that pimozide may improve insulin sensitivity. Accordingly, pimozide treatment produced a mild improvement in insulin tolerance (Figure 2E), though this was not associated with increases in insulin-stimulated Akt and glycogen synthase kinase 3β (GSK3β) phosphorylation in gastrocnemius muscle (Figures S1H and S1I). Notably, the pimozide mediated improvement in glycemia was not due to decreases in body weight or adiposity (Figures S2A and S2B). Likewise, pimozide treatment did not impact food intake or ambulatory activity when housed in metabolic cages (Figures S2C and S2D). Obese mice treated with pimozide also showed no anomalies in circulating triacylglycerol (TAG) or non-esterified fatty acid (NEFA) levels (Figures S2E and S2F), nor did we observe differences in muscle glycogen content (Figure S2G). Indirect calorimetry studies demonstrated that pimozide treatment mildly reduced dark-cycle whole-body oxygen consumption rates and increased the respiratory exchange ratio (RER) (Figures 2F and 2G), which suggests that pimozide-induced reductions in ketone body oxidation increase the muscle's preference for glucose as a fuel source.

Pimozide's Attenuation of Obesity-Induced Hyperglycemia Is Independent of Oxidative Stress, Lipid Accumulation, and Brain SCOT Activity

Obesity-induced hyperglycemia is often associated with muscle oxidative stress and/or lipid accumulation (Muoio and Neufer, 2012; Samuel and Shulman, 2012). However, pimozide treatment had no impact on muscle redox status in obese mice, as reflected by unaltered protein sulfonation levels and reduced/oxidized glutathione ratios (Figures S2H and S2I). Conversely, pimozide treatment decreased gastrocnemius muscle TAG content (Figure 2H), whereas no differences in DAG content nor membrane protein kinase Cθ (PKCθ) levels were observed (Figures S2J and S2K). Unbiased metabolomic profiling also demonstrated negligible changes in numerous acylcarnitine species (Figure S2L). Consistent with a reduction in SCOT activity, β-hydroxybutyrylcarnitine and succinate levels were reduced, whereas succinyl CoA levels were increased via pimozide treatment (Figures 2I–2K). The reductions in gastrocnemius muscle TAG content in response to pimozide treatment were neither associated with increased mRNA expression of enzymes regulating fatty acid metabolism, nor with changes in malonyl CoA content (Figures S2M and S2N). Interestingly, reductions in muscle lipid content were not required for pimozide-mediated improvements in glycemia, as a single acute treatment with pimozide improved glucose tolerance in obese mice without decreasing gastrocnemius TAG content (Figures S2O–S2Q). We conjectured that pimozide-induced glucose lowering arises from inhibiting SCOT in muscle, though it remains possible that pimozide improves glycemia by inhibiting SCOT in other critical ketone body oxidizing tissues, such as the brain, as pimozide was systemically administered. To test whether brain SCOT activity potentially mediates our phenotypes, we performed intracerebroventricular (i.c.v.) injections of pimozide (0.5 μg) in obese C57BL/6J male mice. While acute oral administration of pimozide improved glycemia in obese mice, acute i.c.v. pimozide failed to improve glycemia in these same animals, despite successful inhibition of brain (but not muscle) SCOT activity (Figures 2L–2N). To test that i.c.v. injection of pimozide did not result in its leakage outside the brain, circulating pimozide levels were measured and found to be undetectable (data not shown).

Genetic Inhibition of SCOT Activity in Skeletal Muscle Also Improves Obesity-Induced Hyperglycemia

To further elucidate whether pimozide's salutary actions on obesity-induced hyperglycemia involve a reduction in skeletal muscle ketone body oxidation, we generated skeletal-muscle-specific SCOT knockout ($SCOT^{Muscle-/-}$) mice via crossing floxed SCOT mice with human α-skeletal actin-cre (HSA^{Cre})-expressing mice (Figure S3A). As HSA^{Cre} expression within muscle improves glucose tolerance (Al Batran et al., 2018), we used HSA^{Cre} mice as our respective control littermates and subjected HSA^{Cre} and $SCOT^{Muscle-/-}$ mice to experimental HFD-induced obesity. Intriguingly, obese $SCOT^{Muscle-/-}$ mice almost entirely recapitulated the metabolic phenotype seen with pimozide treatment. More specifically, circulating βOHB levels during overnight fasting were increased in $SCOT^{Muscle-/-}$ mice versus their HSA^{Cre} littermates (Figure 3A), consistent with previous reports (Cotter et al., 2013). $SCOT^{Muscle-/-}$ mice also demonstrated no changes in mRNA expression for genes regulating ketone body utilization in muscle and mRNA expression for genes regulating hepatic ketogenesis (Figure S3B).

With regards to glycemic control, obese $SCOT^{Muscle-/-}$ mice demonstrated a reduction in fasting blood glucose levels (Figure 3B), while glucose tolerance was improved following an overnight fast (Figure 3C), which was associated with reduced circulating insulin levels (Figure 3D). Similarly, insulin-mediated reductions in blood glucose levels were observed during an insulin tolerance test, though this was now associated with mild increases in gastrocnemius muscle Akt but not GSK3β phosphorylation in obese $SCOT^{Muscle-/-}$ mice (Figures 3E and 3F). In contrast to our observations with pimozide, obese $SCOT^{Muscle-/-}$ mice exhibited no differences in whole-body oxygen consumption rates during indirect calorimetry studies, though RER was similarly elevated, suggesting that skeletal muscle glucose oxidation was enhanced in $SCOT^{Muscle-/-}$ mice (Figures 3G and 3H). Further paralleling our observations with pimozide, gastrocnemius muscle protein sulfonation levels and reduced/oxidized glutathione ratios remained similar (Figures S3C and S3D), whereas gastrocnemius TAG content was reduced in obese $SCOT^{Muscle-/-}$ mice (Figure 3I). In addition, no changes were seen regarding DAG content or membrane

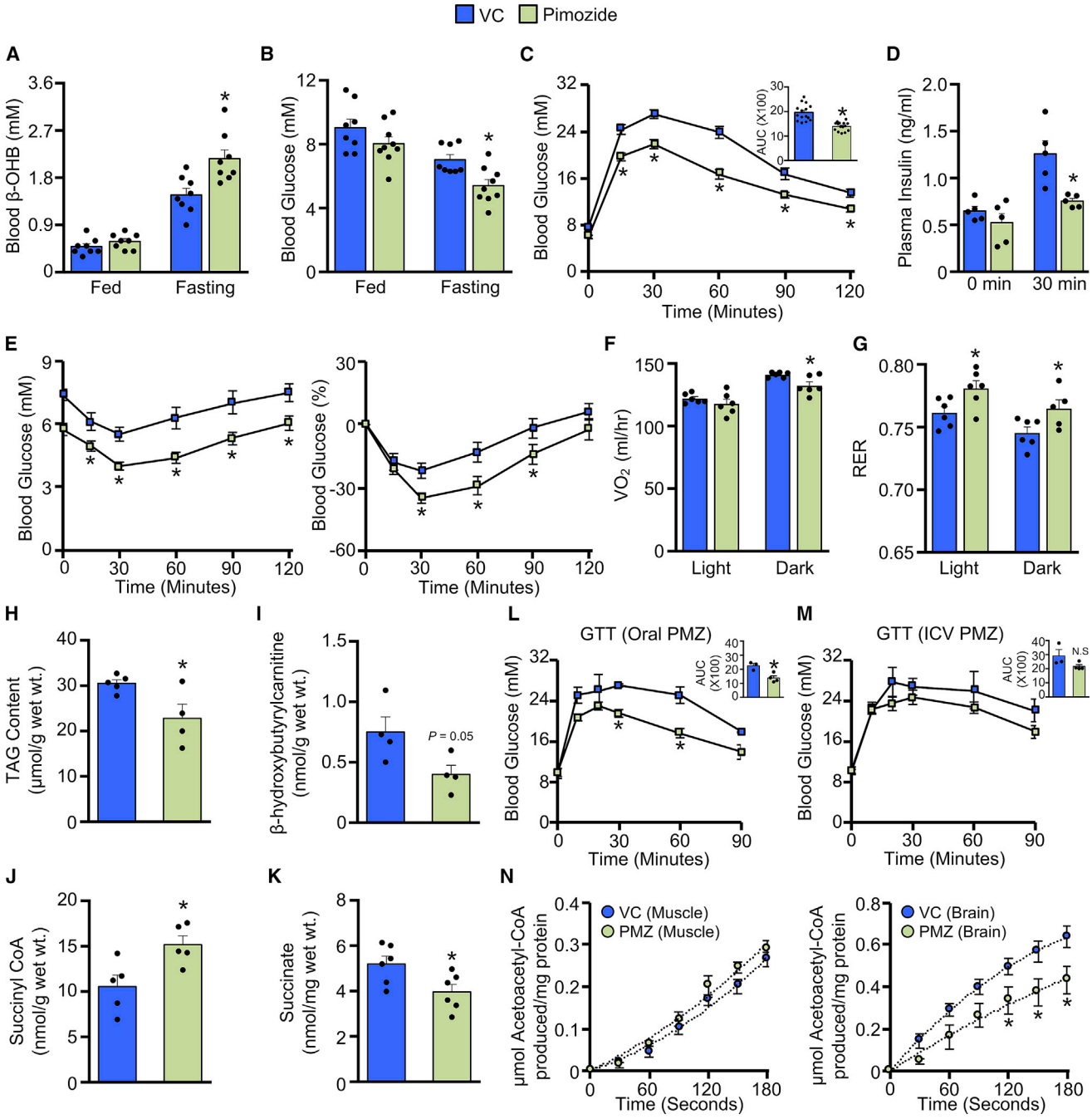

Figure 2. Pimozide Mitigates Obesity-Induced Hyperglycemia

(A and B) Circulating βOHB (n = 8) (A) and blood glucose (n = 8 or 9) (B) levels in obese mice.

(C and D) Glucose tolerance (performed 1 day following the final treatment) (n = 15) (C) and associated circulating plasma insulin levels (n = 5 or 6) (D).

(E–G) Insulin tolerance (performed 1 day following the final treatment) (n = 12) (E) and 24 h whole-body oxygen consumption rates (F) and respiratory exchange ratios (RER) (n = 5) (G).

(H–K) Triacylglycerol (TAG) (n = 5) (H), β-hydroxybutyrylcarnitine (n = 4) (I), succinyl CoA (n = 5) (J), and succinate (n = 6) (K) levels in gastrocnemius muscles from obese mice.

(L–N) Glucose tolerance (GTT) following acute oral (L) or intracerebroventricular (M) administration of VC (n = 3) or pimozide (PMZ) (n = 4) in obese mice, with corresponding gastrocnemius muscle and brain SCOT activity (N).

Values represent means ± SEM. Differences were determined by the use of an unpaired two-tailed Student's t test (C [AUC only], H–L [AUC only], and M [AUC only]) or a two-way ANOVA followed by a Bonferroni post hoc analysis (A–C [GTT only], E–G, L [GTT only], M [GTT only], and N). *$p < 0.05$ versus VC mice. See also Figures S1 and S2.

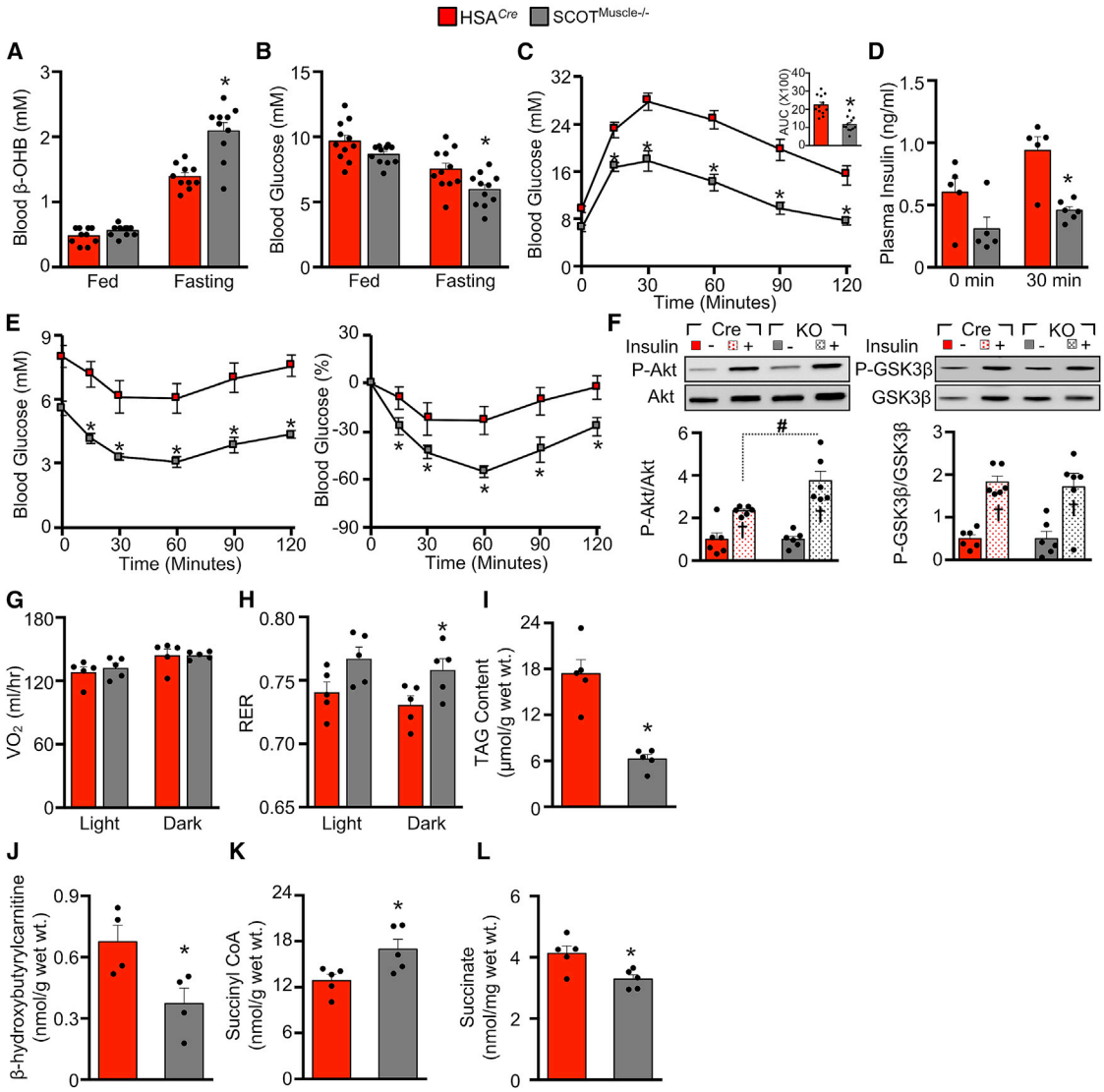

Figure 3. SCOT$^{Muscle-/-}$ Mice Are Protected against Obesity-Induced Hyperglycemia

(A and B) Circulating βOHB (n = 10) (A) and blood glucose (n = 11) (B) levels in obese mice.

(C–F) Glucose tolerance (n = 12) (C), circulating plasma insulin levels (n = 5 or 6) (D), insulin tolerance (n = 12) (E), and associated insulin signaling in gastrocnemius muscles (n = 6) (F).

(G and H) 24 h whole-body oxygen consumption rates (G) and respiratory exchange ratios (RER) (n = 5) (H).

(I–L) Triacylglycerol (TAG) (n = 5) (I), β-hydroxybutyrylcarnitine (n = 4) (J), succinyl CoA (n = 5) (K), and succinate (n = 5) (L) levels in gastrocnemius muscles from obese mice.

Values represent means ± SEM. Differences were determined by the use of an unpaired two-tailed Student's t test or one/two-way ANOVA followed by a Bonferroni post hoc analysis. *$p < 0.05$ versus HSA^{Cre} mice, †$p < 0.05$ versus no insulin counterpart, #$p < 0.05$ versus HSA^{Cre} insulin mice. Cre, HSA^{Cre}; KO, SCOT$^{Muscle-/-}$. See also Figures S2 and S3.

PKCθ expression (Figures S3E and S3F). The reduction in TAG content was once more attributed to neither increased mRNA expression of enzymes regulating fatty acid metabolism nor changes in malonyl CoA content (Figures S3G and S3H), while metabolomic profiling of gastrocnemius muscles demonstrated no changes in numerous acylcarnitine species (Figure S3I). Circulating NEFA levels remained similar, whereas reductions in circulating TAG levels were observed in obese SCOT$^{Muscle-/-}$ mice versus their HSA^{Cre} littermates (Figures S3J and S3K).

Recapitulating our observations with pimozide, reductions in gastrocnemius β-hydroxybutyrylcarnitine levels, succinate levels, and increased succinyl CoA content were observed and reflective of decreased SCOT activity in obese SCOT$^{Muscle-/-}$ mice (Figures 3J–3L). Importantly, the metabolic phenotype of obese SCOT$^{Muscle-/-}$ mice was independent of reductions in body weight, total adiposity, and overall animal activity, though we did note increases in food intake over 24 h during housing in metabolic cages (Figures S3L–S3O). Unexpectedly, the glycemia improvements in obese SCOT$^{Muscle-/-}$ mice did not appear

to involve increases in insulin-stimulated muscle glucose uptake. We observed no differences in muscle glucose uptake rates, whereas glucose infusion rates exhibited trends to mild increases in obese SCOT$^{Muscle-/-}$ mice during hyperinsulinemic-euglycemic clamping studies (Figures S4A–S4E). How such robust improvements in glucose tolerance occur in obese SCOT$^{Muscle-/-}$ mice, or in obese mice treated with pimozide, needs clarification, though changes in non-insulin-mediated glucose uptake (NIMGU) may be involved. In support of this, it has been suggested that 5′AMP-activated protein kinase (AMPK) may be a key mediator of NIMGU (Wiernsperger, 2005), and we observed increased AMPK phosphorylation (indicative of increased AMPK activity) in gastrocnemius muscles from obese SCOT$^{Muscle-/-}$ mice (Figure S4F). As AMPK is also a positive regulator of fatty acid oxidation (Steinberg and Kemp, 2009), it is possible that an increase in AMPK activity contributes to the reduction in muscle TAG content observed in response to SCOT inhibition, despite the absence of changes in gene expression of fatty acid metabolism enzymes.

Pimozide Requires Intact SCOT in Order to Improve Glycemia in Obese Mice

Because obese SCOT$^{Muscle-/-}$ mice phenocopied the glycemia profiles following pimozide treatment, it supports the premise that pimozide alleviates obesity-induced hyperglycemia by decreasing muscle ketone body oxidation secondary to an inhibition of SCOT activity. Nevertheless, to strengthen our conclusions, we repeated our studies in obese SCOT$^{Muscle-/-}$ mice randomized to treatment with either VC or pimozide (10 mg/kg once every 2.5 days via oral gavage) for 2 weeks. Intriguingly, pimozide-induced increases in circulating βOHB levels in overnight fasted obese HSA^{Cre} mice were entirely absent in obese SCOT$^{Muscle-/-}$ mice (Figures 4A and 4B). Furthermore, pimozide reduced gastrocnemius SCOT activity when compared to VC in obese HSA^{Cre} mice (Figure 4C), though the reduction was not as robust as the complete lack of SCOT activity observed in SCOT$^{Muscle-/-}$ mice. Similarly, pimozide-mediated improvements in glucose and insulin tolerance in obese HSA^{Cre} mice were also nonexistent in obese SCOT$^{Muscle-/-}$ mice (Figures 4D and 4E). These results indicate that complete abolishment of SCOT activity in skeletal muscle is not necessary to mitigate obesity-induced hyperglycemia, and they reinforce our data showing that pimozide is a SCOT antagonist. Importantly, agents that target other glucose-lowering mechanisms, such as metformin or the glucagon-like peptide-1 receptor agonist liraglutide, still produced marked improvements in glucose tolerance when administered to obese SCOT$^{Muscle-/-}$ mice (Figures S4G and S4H). This indicates that the lack of improvement following pimozide treatment in obese SCOT$^{Muscle-/-}$ mice is not due to these animals being unable to exhibit any further improvement in glycemia.

Decreasing SCOT Improves Glycemia by Augmenting Skeletal Muscle Pyruvate Dehydrogenase (PDH) Activity

Our studies strongly point to SCOT inhibition as pimozide's glucose lowering mechanism of action, though it remains enigmatic as to how decreases in skeletal muscle SCOT activity and ketone body oxidation yield these potent salutary effects. We hypothesized that increases in glucose oxidation play a role, as both pimozide-treated and SCOT$^{Muscle-/-}$ obese mice were associated with increased RER values (Figures 2H and 3H). In response to HFD-induced obesity, pimozide treatment and SCOT$^{Muscle-/-}$ mice both demonstrated reduced phosphorylation of PDH (rate-limiting enzyme of glucose oxidation) in gastrocnemius muscle, indicative of increased PDH activity (Patel et al., 2014), whereas pimozide failed to further reduce gastrocnemius PDH phosphorylation in obese SCOT$^{Muscle-/-}$ mice (Figure 4F). In addition, refeeding of overnight-fasted lean C57BL/6J mice reduced gastrocnemius PDH phosphorylation, indicative of a transition to increased glucose oxidation, whereas this metabolic flexibility is prevented in mice treated with βOHB at the onset of refeeding and is nullified via concurrent treatment with pimozide (Figure 4G). Illustrating that these observations are due to direct actions on muscle, siRNA knockdown of SCOT in C2C12 myotubes decreased PDH phosphorylation and culture medium lactate levels, reflective of increased glucose oxidation (Figure 4H). Conversely, SCOT overexpression increased PDH phosphorylation and culture medium lactate levels, reflective of decreased glucose oxidation (Figure 4I).

To further highlight the mechanistic importance of increased muscle PDH activity and glucose oxidation as a contributing mechanism to our phenotypes, we generated a new PDH$^{Muscle-/-}$ mouse line and observed that pimozide's ability to improve glucose tolerance was markedly diminished in obese PDH$^{Muscle-/-}$ mice (Figure 4J). Conversely, acute liraglutide treatment was still able to robustly improve glucose tolerance in obese PDH$^{Muscle-/-}$ mice (Figure 4K). The premise that increased muscle PDH activity and glucose oxidation may promote glucose-lowering, is consistent with previous studies whereby whole-body deficiency of *Pdk4* (the kinase that phosphorylates and inhibits PDH activity) in mice improves glycemia during experimental obesity (Jeoung and Harris, 2008). Furthermore, aging is associated with insulin resistance, and lean elderly subjects demonstrated a marked impairment in insulin-stimulated PDH flux versus lean young subjects, indicative of metabolic inflexibility (Petersen et al., 2015). In contrast, lean mice with increased PDH activity via whole-body deficiency of both *Pdk2* and *Pdk4* are insulin resistant in comparison to their lean wild-type littermates, though this is not observed in response to experimental obesity (Rahimi et al., 2014). Despite ongoing debate regarding the role of PDH in regulating glycemia, a mild improvement in glycemia was still observed in obese PDH$^{Muscle-/-}$ mice following pimozide treatment, suggesting that SCOT inhibition may also improve glycemia via alternative mechanisms.

Of interest, another strategy that has been shown to improve glycemia independent of overt improvements in insulin signaling involves a reduction in mitochondrial fatty acid uptake and subsequent overload, thereby decreasing the incomplete oxidation of fatty acids (Koves et al., 2008). Although it remains unknown whether modifying ketone body oxidation will influence the incomplete oxidation of fatty acids, we did not observe any overt lowering of long- and medium-chain acylcarnitine species, suggesting that decreasing ketone body oxidation has no influence on incomplete fatty acid oxidation. Conversely, it has been demonstrated that attenuating mitochondrial overload enhances PDH activity and glucose oxidation (Koves et al., 2008;

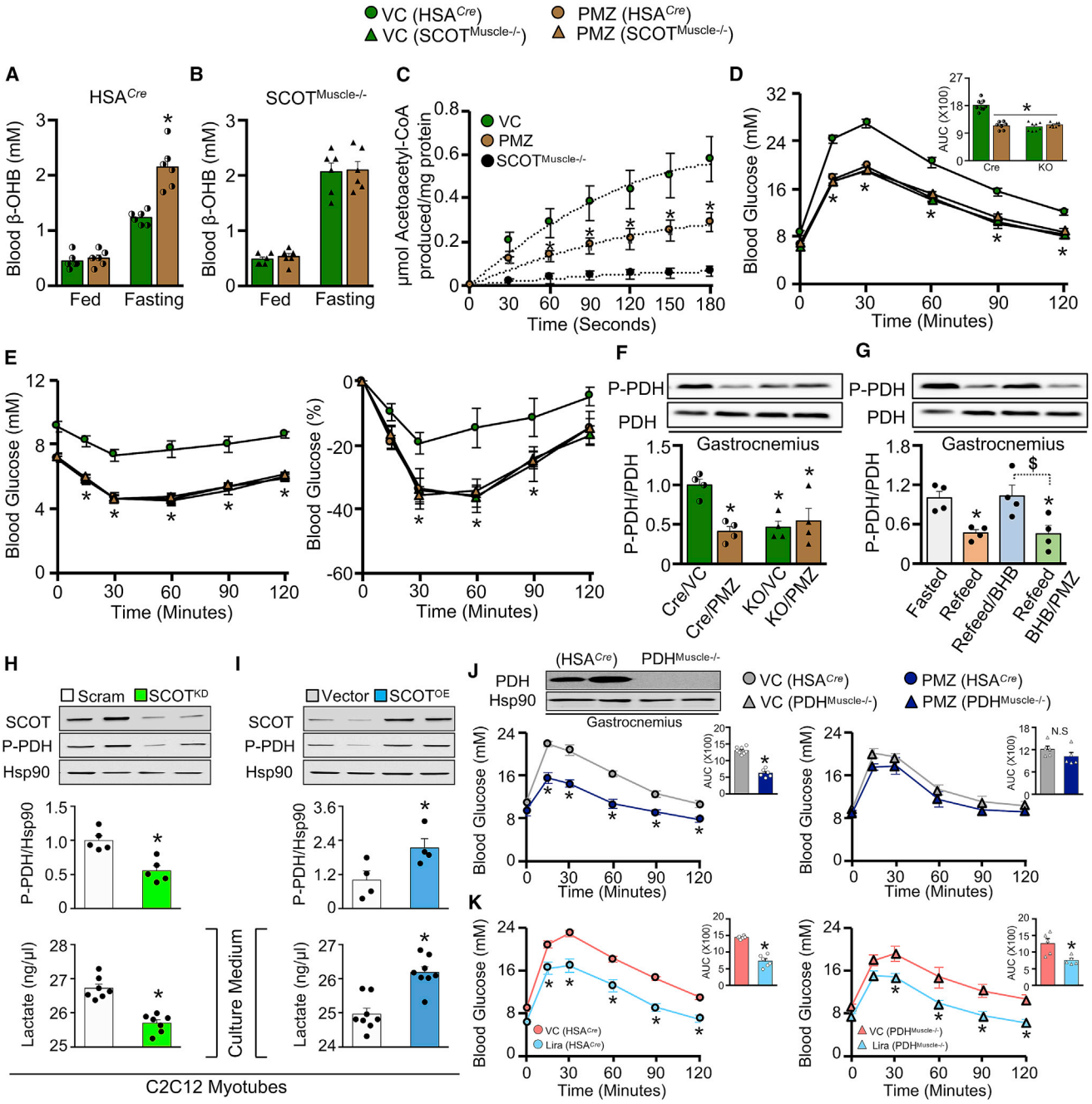

Figure 4. Pimozide Fails to Improve Glycemia in Obese SCOT$^{Muscle-/-}$ Mice and Requires PDH Activity to Promote Glucose Lowering

(A and B) Circulating βOHB levels in obese (A) HSA^{Cre} and (B) SCOT$^{Muscle-/-}$ mice (n = 6).

(C–F) SCOT activity in gastrocnemius muscles (n = 5) (C), glucose tolerance (performed 1 day following the final treatment) and associated AUC (n = 8) (D), insulin tolerance (performed 1 day following the final treatment) (n = 8) (E), and gastrocnemius muscle PDH phosphorylation (n = 4) (F).

(G) Gastrocnemius muscle PDH phosphorylation (n = 4–6) in mice that were fasted, or fasted and refed, with separate cohorts receiving treatment with βOHB or βOHB plus pimozide (PMZ).

(H and I) PDH phosphorylation and culture medium lactate levels (n = 4–6) in C2C12 myotubes following SCOT knockdown (SCOT^{KD}) (H) or SCOT overexpression (SCOT^{OE}) (I). Scram, scramble siRNA.

(J) Immunoblot demonstrating deletion of PDH in gastrocnemius muscles from muscle-specific PDH (PDH$^{Muscle-/-}$) mice, with corresponding glucose tolerance in response to acute PMZ treatment (n = 5–8). Hsp90, heat shock protein 90.

(K) Glucose tolerance in PDH$^{Muscle-/-}$ and HSA^{Cre} mice in response to acute treatment with liraglutide (n = 5 or 6).

Values represent means ± SEM. Differences were determined by the use of an unpaired two-tailed Student's t test or one- or two-way ANOVA followed by a Bonferroni post hoc analysis. *p < 0.05 versus HSA^{Cre} VC group. $p < 0.05 versus refed plus βOHB mice. See also Figure S4.

Muoio et al., 2012), alluding to a potential shared mechanism by which targeting ketone body oxidation and/or incomplete fatty acid oxidation may improve glycemia.

Final Summary and Conclusions

Taken together, our study introduces a number of novel concepts with relation to pharmacological strategies for managing obesity-induced hyperglycemia and/or T2D. Pimozide can reverse many of the detrimental effects of obesity on glucose homeostasis, which appears to stem from pimozide's ability to inhibit skeletal muscle SCOT activity and ketone body oxidation. Our genetic-based studies support this concept, as obese $SCOT^{Muscle-/-}$ mice phenocopied the glucose profiles observed following pimozide treatment. Furthermore, our findings were recapitulated in a mouse model of T2D, as both pimozide treatment and $SCOT^{Muscle-/-}$ mice fed an HFD for 10 weeks with a low-dose injection of streptozotocin (75 mg/kg) at 4 weeks demonstrated significant improvements in glucose tolerance (Figures S4I–S4L). Notably, pimozide failed to further reduce glucose levels in obese $SCOT^{Muscle-/-}$ mice, supporting the notion that pimozide's glucose-lowering mechanism of action requires intact SCOT activity within skeletal muscle.

While our studies allude to SCOT as a novel target of pimozide action, pimozide's clinical utility for suppressing tics in Tourette Syndrome has been attributed to its ability to inhibit dopamine D2 and serotonin 7 receptors (Kossoff and Singer, 2001). As such, these other actions of pimozide will need to be taken into consideration if pimozide is to be considered for the treatment of T2D. Likewise, it will be interesting to determine if pimozide-mediated inhibition of SCOT also contributes to its tic-suppressing actions. Because pimozide is a relatively safe FDA-approved agent with limited toxicities and is readily available on the market (Bruggeman et al., 2001; Sallee et al., 1997), it may potentially allow for quick proof-of-principle clinical studies to confirm whether our observations are translationally reproducible in individuals with obesity with or without T2D. Conversely, since pimozide is able to cross the blood-brain barrier, it may not be the ideal SCOT antagonist to inhibit ketone body oxidation systemically, since the brain relies on ketones as a significant fuel source during prolonged fasting and starvation (Puchalska and Crawford, 2017; Robinson and Williamson, 1980). Rather, we would propose pimozide as the starting point for the development of a new class of drugs that are chemically modified to not cross the blood-brain-barrier, thereby preserving ketone bodies as a physiological fuel source for the brain while inhibiting ketone body oxidation elsewhere in the body (e.g., skeletal muscle) for the treatment of T2D.

Limitations of Study

The marked improvement in glycemia in response to either pharmacological or genetic SCOT inhibition strongly links reductions in skeletal muscle ketone body oxidation to the alleviation of hyperglycemia within the context of the experimental models of obesity, insulin resistance, and T2D studied here. Nonetheless, there are several important limitations that need to be taken into consideration with regards to our study's overall conclusions. As our study was performed exclusively in male mice, it remains unknown whether inhibiting SCOT activity would also improve glucose homeostasis in obese female mice. With regards to increased PDH activity explaining how SCOT inhibition improves glycemia in obesity, we did not measure PDH activity or flux through glucose oxidation in skeletal muscles from mice in our studies. This is potentially important, as PDH can translocate to the nucleus, where it may provide acetyl CoA substrate required for histone acetylation (Sutendra et al., 2014). Hence, it remains possible that the failure of pimozide to improve glycemia in obese $PDH^{Muscle-/-}$ mice is dependent on nuclear PDH activity and not mitochondrial glucose oxidation. Furthermore, we have not yet identified the specific cellular mechanism(s) by which decreasing ketone body oxidation augments PDH activity (e.g., changes in the expression or activity of PDH kinases, PDH phosphatases, etc.). Finally, our pharmacological studies are confined to a 2-week treatment period in obese mice, and we are unable to conclude whether a longer duration of treatment will still yield robust glucose-lowering actions while also being uncertain of what the potential adverse effects of chronically reducing ketone body oxidation are.

STAR★METHODS

Detailed methods are provided in the online version of this paper and include the following:

- KEY RESOURCES TABLE
- RESOURCE AVAILABILITY
  - Lead Contact
  - Materials Availability
  - Data and Code Availability
- EXPERIMENTAL MODEL AND SUBJECT DETAILS
  - Animal Care
  - Generation of Skeletal Muscle-Specific Gene Knockout Mouse Models
  - Intracerebroventricular Cannulation Surgery in Mice
  - Hyperinsulinemic-Euglycemic Clamping Studies
- METHOD DETAILS
  - Isolated Working Heart Perfusions for Assessing Ketone Oxidation
  - Assessment of Glucose Homeostasis
  - Magnetic Resonance Imaging
  - *In Vivo* Metabolic Assessment
  - Blood Chemistry Analysis
  - Pharmacokinetics Assessment of Pimozide
  - Cell Culture
  - Knockdown and Overexpression Studies
  - Virtual High Throughput Screening
  - Mutagenesis
  - Succinyl-CoA:3-ketoacid-CoA Transferase Activity
  - *In Vitro* Kinetics Assessment
  - Western Blotting
  - Real-Time Polymerase Chain Reaction Analysis
  - Determination of Triacylglycerol Content
  - Determination of Diacylglycerol Content
  - Determination of Glycogen Content
  - Metabolomic Profiling
  - Succinyl CoA & Malonyl CoA Content
  - Succinate Assay

SUPPLEMENTAL INFORMATION

Supplemental Information can be found online at https://doi.org/10.1016/j.cmet.2020.03.017.

ACKNOWLEDGMENTS

The HTS molecular modeling studies required access to the Compute Canada and Westgrid online servers. The authors would like to especially thank the dedicated staff working at The Metabolomics Innovation Centre (TMIC), where the metabolomic profiling was carried out. In addition, mass spectrometry work and non-compartmental analysis was provided by the Clinical Pharmacology Analytical Core at Indiana University School of Medicine, a facility supported by the IU Simon Cancer Center Support Grant P30 CA082709. We would also like to thank Christine Bach for her work on method development. Part of this study was conducted at the National Mouse Metabolic Phenotyping Center at UMass Medical School funded by a National Institutes of Health (NIH) grant (5U2C-DK093000). R.A. is a postdoctoral fellow of the Canadian Institutes of Health Research (CIHR) and Diabetes Canada. G.S. is a National New Investigator of the Heart and Stroke Foundation of Canada, J.E.C. is a Borden Scholar, and J.R.U. is a Tier 2 Canada Research Chair (Pharmacotherapy of Energy Metabolism in Obesity). This work was supported by a Career Development Award from the American Diabetes Association (1-18-JDF-017) and an NIH grant (DK123075) to J.E.C., an Allocation Jeune Chercheur from the Société Francophone du Diabète to C.A., and a Project Grant and Foundation Grant to G.S. and J.R.B.D., respectively, from the CIHR.

AUTHOR CONTRIBUTIONS

Conceptualization, R.A. and J.R.U.; Investigation, R.A., K.G., M.E.C., J.J.C., B.S., S.A.T.D., A.A.G., J.N., M.A., N.J.B., G.M., R.K., F.E., E.E.M., L.G., A.R.M., and C.A.; Formal Analysis and Visualization, R.A. and K.G.; Writing – Original Draft, R.A. and J.R.U.; Writing – Review & Editing, R.A., P.A.C., G.S., J.E.C., J.R.B.D., and J.R.U.; Funding Acquisition and Project Administration, J.R.U.; Resources, Z.D., C.V., C.A., P.A.C., G.S., J.E.C., J.R.B.D., and J.R.U.; Supervision, J.R.U. J.R.U. takes full responsibility for the data within this paper.

DECLARATION OF INTERESTS

The University of Alberta has filed a patent application regarding the subject matter of this article.

Received: October 29, 2019
Revised: January 31, 2020
Accepted: March 24, 2020
Published: April 9, 2020

REFERENCES

Aburasayn, H., Al Batran, R., Gopal, K., Almutairi, M., Eshreif, A., Eaton, F., and Ussher, J.R. (2018). Female offspring born to obese and insulin-resistant dams are not at increased risk for obesity and metabolic dysfunction during early development. Can. J. Physiol. Pharmacol. *96*, 97–102.

Al Batran, R., Gopal, K., Martin, M.D., Ho, K.L., Almutairi, M., Aburasayn, H., Eaton, F., Campbell, J.E., and Ussher, J.R. (2018). Skeletal muscle-specific Cre recombinase expression, controlled by the human α-skeletal actin promoter, improves glucose tolerance in mice fed a high-fat diet. Diabetologia *61*, 1849–1855.

Bateman, K.S., Brownie, E.R., Wolodko, W.T., and Fraser, M.E. (2002). Structure of the mammalian CoA transferase from pig heart. Biochemistry *41*, 14455–14462.

Bruggeman, R., van der Linden, C., Buitelaar, J.K., Gericke, G.S., Hawkridge, S.M., and Temlett, J.A. (2001). Risperidone versus pimozide in Tourette's disorder: a comparative double-blind parallel-group study. J. Clin. Psychiatry *62*, 50–56.

Colvin, C.L., and Tankanow, R.M. (1985). Pimozide: use in Tourette's syndrome. Drug Intell. Clin. Pharm. *19*, 421–424.

Cotter, D.G., Schugar, R.C., Wentz, A.E., d'Avignon, D.A., and Crawford, P.A. (2013). Successful adaptation to ketosis by mice with tissue-specific deficiency of ketone body oxidation. Am. J. Physiol. Endocrinol. Metab. *304*, E363–E374.

Cotter, D.G., Ercal, B., Huang, X., Leid, J.M., d'Avignon, D.A., Graham, M.J., Dietzen, D.J., Brunt, E.M., Patti, G.J., and Crawford, P.A. (2014). Ketogenesis prevents diet-induced fatty liver injury and hyperglycemia. J. Clin. Invest. *124*, 5175–5190.

d'Avignon, D.A., Puchalska, P., Ercal, B., Chang, Y., Martin, S.E., Graham, M.J., Patti, G.J., Han, X., and Crawford, P.A. (2018). Hepatic ketogenic insufficiency reprograms hepatic glycogen metabolism and the lipidome. JCI Insight *3*, https://doi.org/10.1172/jci.insight.99762.

DeFronzo, R.A., Ferrannini, E., Groop, L., Henry, R.R., Herman, W.H., Holst, J.J., Hu, F.B., Kahn, C.R., Raz, I., Shulman, G.I., et al. (2015). Type 2 diabetes mellitus. Nat. Rev. Dis. Primers *1*, 15019.

Ellingson, S.R., Smith, J.C., and Baudry, J. (2013). VinaMPI: facilitating multiple receptor high-throughput virtual docking on high-performance computers. J. Comput. Chem. *34*, 2212–2221.

Hall, S.E., Wastney, M.E., Bolton, T.M., Braaten, J.T., and Berman, M. (1984). Ketone body kinetics in humans: the effects of insulin-dependent diabetes, obesity, and starvation. J. Lipid Res. *25*, 1184–1194.

Hirschey, M.D., and Zhao, Y. (2015). Metabolic regulation by lysine malonylation, succinylation, and glutarylation. Mol. Cell. Proteomics *14*, 2308–2315.

Jeoung, N.H., and Harris, R.A. (2008). Pyruvate dehydrogenase kinase-4 deficiency lowers blood glucose and improves glucose tolerance in diet-induced obese mice. Am. J. Physiol. Endocrinol. Metab. *295*, E46–E54.

Kim, H.J., Higashimori, T., Park, S.Y., Choi, H., Dong, J., Kim, Y.J., Noh, H.L., Cho, Y.R., Cline, G., Kim, Y.B., and Kim, J.K. (2004). Differential effects of interleukin-6 and -10 on skeletal muscle and liver insulin action in vivo. Diabetes *53*, 1060–1067.

Kim, M., Astapova, I.I., Flier, S.N., Hannou, S.A., Doridot, L., Sargsyan, A., Kou, H.H., Fowler, A.J., Liang, G., and Herman, M.A. (2017). Intestinal, but not hepatic, ChREBP is required for fructose tolerance. JCI Insight *2*, 96703.

Kossoff, E.H., and Singer, H.S. (2001). Tourette syndrome: clinical characteristics and current management strategies. Paediatr. Drugs *3*, 355–363.

Koves, T.R., Ussher, J.R., Noland, R.C., Slentz, D., Mosedale, M., Ilkayeva, O., Bain, J., Stevens, R., Dyck, J.R., Newgard, C.B., et al. (2008). Mitochondrial overload and incomplete fatty acid oxidation contribute to skeletal muscle insulin resistance. Cell Metab. *7*, 45–56.

Lee, E., Jung, D.Y., Kim, J.H., Patel, P.R., Hu, X., Lee, Y., Azuma, Y., Wang, H.F., Tsitsilianos, N., Shafiq, U., et al. (2015). Transient receptor potential vanilloid type-1 channel regulates diet-induced obesity, insulin resistance, and leptin resistance. FASEB J. *29*, 3182–3192.

Livak, K.J., and Schmittgen, T.D. (2001). Analysis of relative gene expression data using real-time quantitative PCR and the 2(-Delta Delta C(T)) method. Methods *25*, 402–408.

Lopaschuk, G.D., and Ussher, J.R. (2016). Evolving concepts of myocardial energy metabolism: more than just fats and carbohydrates. Circ. Res. *119*, 1173–1176.

Maayah, Z.H., McGinn, E., Al Batran, R., Gopal, K., Ussher, J.R., and El-Kadi, A.O.S. (2019). Role of cytochrome p450 and soluble epoxide hydrolase enzymes and their associated metabolites in the pathogenesis of diabetic cardiomyopathy. J. Cardiovasc. Pharmacol. *74*, 235–245.

Mulvihill, E.E., Varin, E.M., Ussher, J.R., Campbell, J.E., Bang, K.W., Abdullah, T., Baggio, L.L., and Drucker, D.J. (2016). Inhibition of dipeptidyl peptidase-4 impairs ventricular function and promotes cardiac fibrosis in high fat-fed diabetic mice. Diabetes *65*, 742–754.

Muoio, D.M., and Neufer, P.D. (2012). Lipid-induced mitochondrial stress and insulin action in muscle. Cell Metab. *15*, 595–605.

Muoio, D.M., Noland, R.C., Kovalik, J.P., Seiler, S.E., Davies, M.N., DeBalsi, K.L., Ilkayeva, O.R., Stevens, R.D., Kheterpal, I., Zhang, J., et al. (2012). Muscle-specific deletion of carnitine acetyltransferase compromises glucose tolerance and metabolic flexibility. Cell Metab. *15*, 764–777.

Newgard, C.B. (2012). Interplay between lipids and branched-chain amino acids in development of insulin resistance. Cell Metab. *15*, 606–614.

Patel, M.S., Nemeria, N.S., Furey, W., and Jordan, F. (2014). The pyruvate dehydrogenase complexes: structure-based function and regulation. J. Biol. Chem. *289*, 16615–16623.

Petersen, K.F., Morino, K., Alves, T.C., Kibbey, R.G., Dufour, S., Sono, S., Yoo, P.S., Cline, G.W., and Shulman, G.I. (2015). Effect of aging on muscle mitochondrial substrate utilization in humans. Proc. Natl. Acad. Sci. USA *112*, 11330–11334.

Puchalska, P., and Crawford, P.A. (2017). Multi-dimensional roles of ketone bodies in fuel metabolism, signaling, and therapeutics. Cell Metab. *25*, 262–284.

Rahimi, Y., Camporez, J.P., Petersen, M.C., Pesta, D., Perry, R.J., Jurczak, M.J., Cline, G.W., and Shulman, G.I. (2014). Genetic activation of pyruvate dehydrogenase alters oxidative substrate selection to induce skeletal muscle insulin resistance. Proc. Natl. Acad. Sci. USA *111*, 16508–16513.

Robinson, A.M., and Williamson, D.H. (1980). Physiological roles of ketone bodies as substrates and signals in mammalian tissues. Physiol. Rev. *60*, 143–187.

Ruderman, N.B., and Goodman, M.N. (1973). Regulation of ketone body metabolism in skeletal muscle. Am. J. Physiol. *224*, 1391–1397.

Saleme, B., Gurtu, V., Zhang, Y., Kinnaird, A., Boukouris, A.E., Gopal, K., Ussher, J.R., and Sutendra, G. (2019). Tissue-specific regulation of p53 by PKM2 is redox dependent and provides a therapeutic target for anthracycline-induced cardiotoxicity. Sci. Transl. Med. *11*, https://doi.org/10.1126/scitranslmed.aau8866.

Sallee, F.R., Pollock, B.G., Stiller, R.L., Stull, S., Everett, G., and Perel, J.M. (1987). Pharmacokinetics of pimozide in adults and children with Tourette's syndrome. J. Clin. Pharmacol. *27*, 776–781.

Sallee, F.R., Nesbitt, L., Jackson, C., Sine, L., and Sethuraman, G. (1997). Relative efficacy of haloperidol and pimozide in children and adolescents with Tourette's disorder. Am. J. Psychiatry *154*, 1057–1062.

Samuel, V.T., and Shulman, G.I. (2012). Mechanisms for insulin resistance: common threads and missing links. Cell *148*, 852–871.

Steinberg, G.R., and Kemp, B.E. (2009). AMPK in health and disease. Physiol. Rev. *89*, 1025–1078.

Sung, M.M., Kim, T.T., Denou, E., Soltys, C.M., Hamza, S.M., Byrne, N.J., Masson, G., Park, H., Wishart, D.S., Madsen, K.L., et al. (2017). Improved glucose homeostasis in obese mice treated with resveratrol is associated with alterations in the gut microbiome. Diabetes *66*, 418–425.

Sutendra, G., Kinnaird, A., Dromparis, P., Paulin, R., Stenson, T.H., Haromy, A., Hashimoto, K., Zhang, N., Flaim, E., and Michelakis, E.D. (2014). A nuclear pyruvate dehydrogenase complex is important for the generation of acetyl-CoA and histone acetylation. Cell *158*, 84–97.

Ussher, J.R., Jaswal, J.S., Wagg, C.S., Armstrong, H.E., Lopaschuk, D.G., Keung, W., and Lopaschuk, G.D. (2009a). Role of the atypical protein kinase Czeta in regulation of 5′-AMP-activated protein kinase in cardiac and skeletal muscle. Am. J. Physiol. Endocrinol. Metab. *297*, E349–E357.

Ussher, J.R., Koves, T.R., Jaswal, J.S., Zhang, L., Ilkayeva, O., Dyck, J.R., Muoio, D.M., and Lopaschuk, G.D. (2009b). Insulin-stimulated cardiac glucose oxidation is increased in high-fat diet-induced obese mice lacking malonyl CoA decarboxylase. Diabetes *58*, 1766–1775.

Ussher, J.R., Koves, T.R., Cadete, V.J., Zhang, L., Jaswal, J.S., Swyrd, S.J., Lopaschuk, D.G., Proctor, S.D., Keung, W., Muoio, D.M., and Lopaschuk, G.D. (2010). Inhibition of de novo ceramide synthesis reverses diet-induced insulin resistance and enhances whole-body oxygen consumption. Diabetes *59*, 2453–2464.

Ussher, J.R., Folmes, C.D., Keung, W., Fillmore, N., Jaswal, J.S., Cadete, V.J., Beker, D.L., Lam, V.H., Zhang, L., and Lopaschuk, G.D. (2012a). Inhibition of serine palmitoyl transferase I reduces cardiac ceramide levels and increases glycolysis rates following diet-induced insulin resistance. PLoS One *7*, e37703.

Ussher, J.R., Wang, W., Gandhi, M., Keung, W., Samokhvalov, V., Oka, T., Wagg, C.S., Jaswal, J.S., Harris, R.A., Clanachan, A.S., et al. (2012b). Stimulation of glucose oxidation protects against acute myocardial infarction and reperfusion injury. Cardiovasc. Res. *94*, 359–369.

Ussher, J.R., Baggio, L.L., Campbell, J.E., Mulvihill, E.E., Kim, M., Kabir, M.G., Cao, X., Baranek, B.M., Stoffers, D.A., Seeley, R.J., and Drucker, D.J. (2014). Inactivation of the cardiomyocyte glucagon-like peptide-1 receptor (GLP-1R) unmasks cardiomyocyte-independent GLP-1R-mediated cardioprotection. Mol. Metab. *3*, 507–517.

Verma, S., Rawat, S., Ho, K.L., Wagg, C.S., Zhang, L., Teoh, H., Dyck, J.E., Uddin, G.M., Oudit, G.Y., Mayoux, E., et al. (2018). Empagliflozin increases cardiac energy production in diabetes: novel translational insights into the heart failure benefits of SGLT2 inhibitors. JACC Basic Transl. Sci. *3*, 575–587.

Vice, E., Privette, J.D., Hickner, R.C., and Barakat, H.A. (2005). Ketone body metabolism in lean and obese women. Metabolism *54*, 1542–1545.

Wiernsperger, N.F. (2005). Is non-insulin dependent glucose uptake a therapeutic alternative? Part 1: physiology, mechanisms and role of non insulin-dependent glucose uptake in type 2 diabetes. Diabetes Metab. *31*, 415–426.

STAR★METHODS

KEY RESOURCES TABLE

REAGENT or RESOURCE	SOURCE	IDENTIFIER
Antibodies		
Rabbit polyclonal anti-SCOT	ProteinTech	Cat# 12175-1-AP; RRID: AB_2157444
Goat polyclonal anti-ACAT1	Thermo Fisher Scientific	Cat# PA5-19227; RRID: AB_10977900
Mouse monoclonal anti-Hsp90	BD Biosciences	Cat# 610418; RRID: AB_397798
Rabbit polyclonal anti-succinyllysine	PTM Biolabs	Cat# PTM-401; RRID: AB_2687628
Rabbit polyclonal anti-AKT	Cell Signaling Technology	Cat# 9272; RRID: AB_329827
Rabbit polyclonal anti-phospho-Akt (Ser473)	Cell Signaling Technology	Cat# 4060; RRID: AB_2315049
Rabbit monoclonal anti-GSK-3alpha/beta (D75D3)	Cell Signaling Technology	Cat# 5676; RRID: AB_10547140
Rabbit polyclonal anti-phospho-GSK-3alpha/beta (Ser21/9)	Cell Signaling Technology	Cat# 9331; RRID: AB_329830
Rabbit monoclonal anti-PDHA1	Cell Signaling Technology	Cat# 3205; RRID: AB_2162926
Rabbit polyclonal anti-phospho-PDHE1-A type I (Ser293)	Millipore	Cat# ABS204; RRID: AB_11205754
Rabbit monoclonal anti-AMPK (D63G4)	Cell Signaling Technology	Cat# 5832; RRID: AB_10624867
Rabbit monoclonal anti-phospho-AMPK (Thr172)	Cell Signaling Technology	Cat# 2535; RRID: AB_331250
Rabbit polyclonal anti-Na^+/K^+ ATPase alpha	Cell Signaling Technology	Cat# 3010; RRID: AB_2060983
Rabbit monoclonal anti-PKCθ (E1I7Y)	Cell Signaling Technology	Cat# 13643; RRID: AB_2798282
Anti-rabbit IgG, HRP-linked antibody	Cell Signaling Technology	Cat# 7074; RRID: AB_2099233
Anti-mouse IgG, HRP-linked antibody	Cell Signaling Technology	Cat# 7076; RRID: AB_330924
Anti-goat IgG, HRP-linked antibody	Thermo Fisher Scientific	Cat# A15963; RRID: AB_2534637
Bacterial and Virus Strains		
DH5α competent cells	Thermo Fisher Scientific	Cat# 18258012
Chemicals, Peptides, and Recombinant Proteins		
SCOT1 recombinant protein	MyBiosource	Cat# MBS9420519
Pimozide	Sigma-Aldrich	Cat# 2062784
Insulin (Humulin)	Eli Lilly and Co.Bio	Cat# VL7510
Succinyl-CoA	Sigma	Cat# 108347973
Lithium acetoacetate	Sigma	Cat# 3483112
Critical Commercial Assays		
Triacylglycerol Assay Kit	FUJIFILM Wako Diagnostics U.S.A	Cat# 994-02891, 992-02892, 464-01601, 416-00102
Succinate Assay	Abcam	Cat# Ab204718
GSH/GSSG Ratio Detection Assay Kit	Abcam	Cat# Ab138881
Ultrasensitive Mouse Insulin ELISA Kit	ALPCO	Cat# 80-INSMSU-E01
Diacylglycerol Assay Kit	Abcam	Cat# Ab242293
Experimental Models: Cell Lines		
Mouse: C2C12 cell line	ATCC	Cat# CRL-1772
Experimental Models: Organisms/Strains		
C57BL/6J mice	In-house colony at the University of Alberta	N/A
Floxed *Oxct1*	Mice provided via Dr. Peter Crawford	N/A
Floxed *Pdha1*	Jackson Laboratory	Stock # 017443
HSA-MerCreMer	Jackson Laboratory	Stock # 025750

(*Continued on next page*)

Continued

REAGENT or RESOURCE	SOURCE	IDENTIFIER
Oligonucleotides		
siRNA SMART Pool ON-TARGET *Oxct1*	Dharmacon	Cat# 67041
Mouse *Oxct1* Ile323Ala mutagenesis primer (forward) 5′AGAAGAGGAATCCCAGCACCCAAGTTAGCGT ACATGCCG3′; 5′CGGCATGTACGCTAACTTGGG TGCTGGGATTCCTCTTCT3′ (reverse)	Integrated DNA Technologies	Custom synthesis
Mouse *Oxct1* Lys368Ala mutagenesis primer (forward) 5′GAACAGTAACTGTTTCCGCTCCTGCATTGATGA GATCCGC3′; 5′GCGGATCTCATCAATGCAGGA GCGGAAACAGTTACTGTTC3′(reverse)	Integrated DNA Technologies	Custom synthesis
Mouse *Acat1*	Thermo Fisher Scientific	Cat# Mm00507463_m1
Mouse *Bdh1*	Thermo Fisher Scientific	Cat# Mm00558330_m1
Mouse *Bdh2*	Thermo Fisher Scientific	Cat# Mm00459075_m1
Mouse *Oxct1*	Thermo Fisher Scientific	Cat# Mm00499303_m1
Mouse *Hmgcs2*	Thermo Fisher Scientific	Cat# Mm00550050_m1
Mouse *Acadm*	Thermo Fisher Scientific	Cat# Mm01323360_g1
Mouse *Acox1*	Thermo Fisher Scientific	Cat# Mm01246834_m1
Mouse *Ppia*	Thermo Fisher Scientific	Cat# Mm02342430_g1
Recombinant DNA		
Human *OXCT1*	Sino Biological	Cat# HG15008-UT
pFLAG-CMV-5b vector	Sigma	Cat# E7648
Software and Algorithms		
ImageJ		https://imagej.nih.gov/ij/
Prism 6	GraphPad	https://www.graphpad.com/scientific-software/prism/
Other		
[U-^{14}C]β-hydroxybutyrate	American Radiolabeled Chemicals	ARC 1545
Low-fat diet (10% kcal from lard)	Research Diets	D12450J
High-fat diet (60% kcal from lard)	Research Diets	D12492

RESOURCE AVAILABILITY

Lead Contact

Further information and requests for resources and reagents should be directed to the Lead Contact for this manuscript, John Ussher (jussher@ualberta.ca).

Materials Availability

This study did not generate any new materials.

Data and Code Availability

This study did not generate/analyze any datasets/code.

EXPERIMENTAL MODEL AND SUBJECT DETAILS

Animal Care

All animals received care according to the guidelines from the Canadian Council on Animal Care, and all animal procedures were approved by the institution's Health Sciences Animal Welfare Committee. Animal husbandry consisted of all mice being housed at 22°C in a 12 h light and 12 h dark cycle (lights on from 6 am to 6 pm), with all mice receiving standard environmental enrichment (chip bedding, a plastic tube, 8 ounces of crinkle paper, and Nestlet square bedding comprised of short fiber cotton) and *ad libitum* access to food and water. 6 – 8-week-old male mice were either fed a standard chow, low-fat diet (10% kcal from lard, D12450J); or a high-fat diet (60% kcal from lard, Research Diets; D12492) for 10 weeks to induce obesity. At the age of 16 – 18 weeks, animals were killed via intraperitoneal (IP) injection of sodium pentobarbital (12 mg) in the fed state in the middle of the dark cycle, for the extraction of tissues (e.g., gastrocnemius muscles, liver, etc.) that were immediately frozen in liquid nitrogen with Wollenberger tongs and stored

at −80°C. In a separate cohort of obese male mice, animals were randomized to receive treatment with either vehicle control (VC;corn oil) or pimozide (10 mg/kg once every 2.5 days) via oral gavage for 2 weeks. Upon study completion, all animals were killed following an overnight fast and at 30 min post-administration of saline or insulin, or in the middle of the dark cycle after a 2 h or overnight fast, for the extraction of tissues that were immediately snap frozen in liquid nitrogen with Wollenberger tongs and stored at −80°C. Separate cohorts of obese male mice were treated 1x with VC or pimozide (10 mg/kg) and killed upon completion of a glucose tolerance test following an overnight fast, following which their livers and muscles were immediately extracted and snap frozen in liquid nitrogen using Wollenberger tongs and stored at −80°C. Last, a cohort of lean C57BL/6J male mice were fasted overnight, following which the mice either remain fasted for an additional 2 h, or were refed for 2 h, with or without treatment of β-hydroxybutyrate (βOHB, 1.5 g/kg), or βOHB and pimozide (10 mg/kg). The mice were subsequently killed and gastrocnemius muscles were extracted and immediately snap frozen in liquid nitrogen with Wollenberger tongs and stored at −80°C.

To induce experimental type 2 diabetes (T2D) in mice, we followed a similar protocol as described above involving 10 weeks supplementation of a high-fat diet, but also administered a single low-dose injection of streptozotocin (75 mg/kg) at 4 weeks as previously described (Maayah et al., 2019; Mulvihill et al., 2016). Animals were then randomized to receive treatment with either VC (corn oil) or pimozide (10 mg/kg once every 2.5 days) via oral gavage for 2 weeks. Upon study completion all animals were killed following an overnight fast, for the extraction of tissues that were immediately snap frozen in liquid nitrogen with Wollenberger tongs and stored at −80°C. Importantly, we have demonstrated that use of this experimental T2D model produces a further worsening of glycemia versus experimental obesity, while also producing diastolic dysfunction (Maayah et al., 2019).

Generation of Skeletal Muscle-Specific Gene Knockout Mouse Models

Female homozygous floxed succinyl-CoA:3-ketoacid-CoA transferase (SCOT) or homozygous floxed pyruvate dehydrogenase (PDH) mice (The Jackson Laboratory, Stock no. 017443) were crossed with male heterozygous human α-skeletal actin-Cre (HSA^{Cre}) expressing mice (The Jackson Laboratory, Stock no. 025750). Male offspring heterozygous for HSA^{Cre} and heterozygous for floxed SCOT or floxed PDH were subsequently crossed with female offspring heterozygous for floxed SCOT or floxed PDH, in order to generate skeletal muscle-specific SCOT knockout ($SCOT^{Muscle-/-}$) mice or skeletal muscle-specific PDH knockout ($PDH^{Muscle-/-}$) mice, respectively. 6-week-old HSA^{Cre} and $SCOT^{Muscle-/-}$ or $PDH^{Muscle-/-}$ male mice received daily IP injections of tamoxifen (50 mg/kg) suspended in corn oil for 5 days, following which all mice were allowed a one week washout post-tamoxifen. 8-week-old HSA^{Cre} and $SCOT^{Muscle-/-}$ or $PDH^{Muscle-/-}$ male mice were subsequently fed a low-fat diet (10% kcal from lard, D12450J); or high-fat diet (60% kcal from lard, Research Diets; D12492) for 10 weeks to induce obesity. At 9 weeks and 10 weeks post-diet supplementation, all mice underwent glucose tolerance testing and insulin tolerance testing, respectively. At study completion, all animals were killed following an overnight fast and at 30 min post-administration of saline or insulin, or in the middle of the dark cycle, for the extraction of tissues that were immediately snap frozen in liquid nitrogen with Wollenberger tongs and stored at −80°C. In specific cohorts of 8-week-old HSA^{Cre} and $SCOT^{Muscle-/-}$ male mice, after being subjected to high-fat diet-induced obesity for 10 weeks, the animal's drinking water was supplemented with either VC or metformin (400 mg/kg per day) for 2 weeks, or animals received an acute subcutaneous treatment with either VC or liraglutide (30 μg/kg) prior to the assessment of glucose tolerance in response to a 6 h fast.

Intracerebroventricular Cannulation Surgery in Mice

8-week-old C57BL/6J male mice were fed a high-fat diet (60% kcal from lard, Research Diets; D12492) for 5 weeks prior to undergoing intracerebroventricular cannulation surgery, and housed at room temperature in a 12 h light and 12 h dark cycle (lights on from 7 am to 7 pm) with *ad libitum* access to food and water. All mice are anesthetized with a table-top isoflurane laboratory anesthesia system (3% isoflurane; O_2 flow of 2 L/min for the induction of anesthesia, anesthetic nose cone is used to maintain anesthesia with isoflurane concentration of ~1%–2% and O_2 flow of 2 l/min). Once surgical anesthesia is reached and the mouse undergoes a surgical scrub, the mouse is immobilized in a stereotaxic apparatus (David Kopf, Tujunga, CA, USA). An incision is subsequently made on the head to expose the skull, and a stereotaxic frame-mounted drill was used to make a bore hole (< 1 mm in diameter). A small screw (Plastics One, 2.4 mm shaft length, 1.57 shaft diameter) is implanted to the skull region around the hole which was prepared for the implantation. A stainless-steel guide cannula (Plastics One, C315GS-2/SPC, 26 GA, PED 2 mm) with a small dummy cannula (Plastics One, C315FDS-2/SPC, diameter 0.008," PED 2 mm) is then inserted into the guide cannula, which is lowered slowly to minimize brain damage and bleeding into the brain to a position immediately above the target region. The stereotactic coordinates for the lateral ventricle at AP = 0.2 mm, ML = 1.0 mm and DV = −1.5 mm (final internal tip positions from brain surface). The cannula and immediate surrounding regions are then coated with Vetbond Tissue Adhesive (3M, for animals), and the cannula is held in place on the skull using dental cement (Parkell, NY, US). Wound margins are closed with subcutaneous interrupted stitch 4-0 absorbable suture if needed.

Following successful surgery all mice are individually housed with *ad libitum* access to food and water and allowed a 1-week recovery period prior to experimentation. For the intra-brain administration of pimozide, mice are first subjected to anesthesia in an anesthesia induction box (3% isoflurane and O_2 flow of 2 l/min). Once deep anesthesia is confirmed by a lack of whisker and toe-pinch reflex, mice are quickly moved to an operating area, following which the dummy cannula is quickly removed from the previously implanted guide cannula, and an infusion internal cannula (Plastics One, 33GA, 2mm Ped) is inserted into the target site through the guide cannula. This operation is completed within 10 s and the animals are then returned to their original cage. The infusion internal cannula is connected by MicroRenathane tubing (Braintree Scientific, Braintree, MA, USA) to a 5 mL BD syringe

before the start of the animal's operation, and after the animals recover from the anesthesia, the injections are made over 1 μl/min by a Programmable Syringe Pump (Braintree scientific, USA). Pimozide was dissolved in dimethylsulfoxide (DMSO) and diluted to a final concentration of 10% dimethylsulfoxide (DMSO) in artificial cerebrospinal fluid, and 0.5 μg of pimozide was administered to the mouse via the Programmable Syringe Pump.

Hyperinsulinemic-Euglycemic Clamping Studies

Obese HSA^{Cre} and $SCOT^{Muscle-/-}$ mice underwent survival surgery 5 or 6 days prior to undergoing a hyperinsulinemic-euglycemic clamp, to establish an indwelling catheter in the jugular vein as previously described (Kim et al., 2004). On the day of the clamp experiment, all mice were fasted (6 h) with free access to water, and a 2 h clamp was conducted in conscious mice with a primed and continuous infusion of human insulin (150 mU/kg body weight followed by 2.5 mU/kg per minute; Humulin; Eli Lilly, Indianapolis, IN, USA) as previously described (Lee et al., 2015). In order to maintain euglycemia, 20% glucose was infused at variable rates during the clamp. Whole-body glucose turnover was quantified with a continuous infusion of [3-^{3}H]glucose (PerkinElmer, Waltham, MA, USA), and 2-deoxy-d-[1-^{14}C]glucose was administered as a bolus (10 μCi) 75 min after the start of the clamp experiment, to measure insulin-stimulated glucose uptake in various organs (e.g., gastrocnemius muscle). All mice were killed at the end of the clamp for tissue collection as previously described (Lee et al., 2015).

METHOD DETAILS

Isolated Working Heart Perfusions for Assessing Ketone Oxidation

Mice were anaesthetized via IP injection of sodium pentobarbital (60 mg/kg), and hearts were subsequently excised and immersed in ice-cold Krebs-Henseleit bicarbonate solution, following which the aorta was cannulated and equilibrated in the Langendorff mode. Hearts were subsequently switched to and perfused in the working mode as previously described (Ussher et al., 2012a, 2012b). Oxygenated Krebs-Henseleit solution consisting of 0.8 mM [9,10-^{3}H] palmitate bound to 3% fatty acid free bovine serum albumin, 5.0 mM glucose and 0.8 mM [U-^{14}C]βOHB was delivered to the left atrium at a preload pressure of 15 mmHg, while perfusate was ejected from hearts into the aortic outflow line against a hydrostatic afterload pressure of 50 mmHg. Hearts were perfused aerobically for 40 min and βOHB oxidation was assessed as previously described (Verma et al., 2018). At the end of perfusion, hearts were immediately snap frozen in liquid nitrogen with Wollenberger tongs and stored at −80°C.

Assessment of Glucose Homeostasis

Glucose and insulin tolerance tests were performed in mice fasted overnight or after a 6 h fast, following which IP glucose (2 g/kg) or insulin (0.5 U/kg) was administered. Blood glucose measurements were assessed via tail whole-blood at the end of the fast (0 min), followed by samples at 15, 30, 60, 90, and 120 min post-glucose or insulin administration, using the Contour Next blood glucose monitoring system (Bayer). Plasma was also collected during the glucose tolerance test from tail whole-blood at the 0 and 15 min time points for the assessment of circulating insulin levels, using a commercially available enzyme-linked immunosorbent assay kit (Alpco Diagnostics) according to the manufacturer's instructions. In brief, 5 μL of each sample was added to each well with 75 μL of a provided enzyme conjugate, and the 96 well plate was then incubated for 2 h at room temperature on an orbital microplate shaker at ~700-900 RPM. After incubation, the plate was washed 6x with a provided working strength wash buffer, and then 100 μL of a provided substrate was added to each well to start the reaction, which was terminated after 30 min via addition of 100 μL of stop solution. Any air bubbles were removed and plasma insulin levels "ng/mL" were determined via reading the absorbance of the plate at a wavelength of 450 nm.

Magnetic Resonance Imaging

Mice underwent assessment of body composition via quantitative nuclear magnetic resonance relaxometry to quantify total lean/fat mass utilizing an EchoMRI-4in1/700 body composition analyzer as previously described (Aburasayn et al., 2018).

In Vivo Metabolic Assessment

In vivo metabolic assessment via indirect calorimetry was performed using the Oxymax comprehensive laboratory animal monitoring system (Columbus Instruments). Animals with *ad libitum* access to food and water were initially acclimatized in the system for a 24 h period. The subsequent 24 h period was utilized for data collection as previously described (Aburasayn et al., 2018). During indirect calorimetry, animal activity, food and water intake, whole-body O_2 consumption rates, heat production, and respiratory exchange ratios were quantified.

Blood Chemistry Analysis

Measurement of blood glucose (Contour Next (Bayer)), βOHB (FreeStyle Precision Blood β-ketone, Abbott Laboratories) and lactate (Lactate Plus Meter, Nova Biomedical) levels were performed in tail whole-blood samples obtained during the random fed state or following an overnight fast.

Pharmacokinetics Assessment of Pimozide

Pimozide and lidoflazine were purchased from Sigma Aldrich Chemical Co. (St Louis, MO). Methanol, acetonitrile, ethyl acetate, ammonium acetate, and glacial acetic acid were purchased from Fisher Scientific (Fairlawn, NJ). All solvents were high-performance liquid chromatography (HPLC) grade. Deionized water was purified using a Barnstead GenPure UV/UF xCAD plus water system (Thermo Fisher Scientific, Waltham, MA). Mouse plasma (CD-1, pooled gender) for plasma standard and quality control preparations was purchased from BioIVT (Hicksville, NY). Naive tissue for tissue standard preparations was generously gifted by the *In Vivo* Therapeutics Core (Indiana Melvin and Bren Simon Cancer Center, Indianapolis, IN).

Plasma pimozide and lidoflazine (internal standard) was quantified by HPLC-MS/MS (5500 QTRAP AB Sciex, Framingham, MA). In brief, pimozide and lidoflazine were separated by a gradient mobile phase (acetonitrile: 5mM NH_4OAc; pH = 3.5) with an Agilent Zorbax 300SB-C8 150X4.6 mm 5 μm column. The mass spectrometer (MS/MS) utilized an electrospray ionization probe run in positive mode. The multiple reaction monitoring (MRM) Q1/Q3 (m/z) transitions for pimozide and lidoflazine were 462.2/109.2 and 492.3/343.2, respectively. For the plasma samples, 20 μL per sample was transferred to a polypropylene tube, lidoflazine was added as the internal standard (20 μL of 0.01 ng/μL), and the extraction was performed by the addition of 0.1M citric acid buffer (pH 3.0) followed by the addition of ethyl acetate. The samples were then vortex mixed, centrifuged and the organic layer was transferred to a clean polypropylene tube and evaporated to dryness. The samples were then reconstituted with methanol (50 μL) and an aliquot (10 μL) was injected into the HPLC-MS/MS. The lower limit of quantification was 0.1 ng/mL. The standard curve was linear from 0.1 – 1,000 ng/mL.

Pimozide was quantified from tissue (brain and muscle) samples using a slightly modified method from the plasma sample analysis described above. Briefly, the tissue was weighed and then transferred to a polypropylene tube. Phosphate buffered saline (PBS) was added to the tissue to bring the total volume to 1 mL (assumption 1 g = 1 mL). The tissue was homogenized using a TissueRuptor with a single use disposable probe. An aliquot (0.8 mL) was transferred to a clean polypropylene tube and lidoflazine was added as the internal standard (20 μL of 0.1 ng/μL). The extraction procedure and HPLC-MS/MS conditions were the same as for the plasma samples. The lower limit of quantification was 0.08 ng/sample. The standard curve was linear from 0.08 – 240 ng/sample.

Non-compartmental pharmacokinetics analysis was performed using PK solver add-in program in Microsoft Excel (2016). Pharmacokinetic parameters included: $t_{1/2}$ (half-life, $t_{1/2} = 0.693/k_{el}$) C_{max} (maximal plasma concentration), t_{max} (time of maximal plasma concentration), $AUC_{0-\infty}$ (area under the plasma concentration time curve from zero to infinity), V_d (volume of distribution calculated by clearance/mean residence time), apparent oral clearance (calculated by (CL/F) = dose/AUC).

Cell Culture

All reagents were obtained from Sigma. C2C12 cells (American Type Culture Collection; female origin) were cultured in 6-well plates in Dulbecco's modified Eagle's medium (DMEM) containing 10% fetal bovine serum (FBS) and 1% penicillin/streptomycin. Cells were incubated in a water-jacketed CO_2 incubator maintained at 37°C with 5% CO_2. Upon confluency C2C12 cells were differentiated into myotubes via growth in DMEM containing 2% horse serum and 1% penicillin/streptomycin as previously described (Ussher et al., 2009a). C2C12 myotubes were cultured in glucose free DMEM supplemented with 0.4 mM oleate bound to 2% bovine serum albumin (BSA), 5.0 mM glucose, 0.6 mM βOHB, 0.25 mM L-carnitine and 0.2 nM insulin for 24 h.

Knockdown and Overexpression Studies

Knockdown of SCOT in C2C12 myotubes was carried out using SMART Pool ON-TARGET Plus, a mixture of 4 siRNAs against SCOT provided as a single reagent, (Dharmacon, 67041). C2C12 myotubes were transfected with a scramble siRNA sequence, or mouse SCOT siRNA for 48 h using Lipofectamine RNAiMAX (Thermo Scientific) as per manufacturer's instructions. On the contrary, overexpression of SCOT was accomplished via transfection of C2C12 myotubes with pCMV vector or vector expressing the Human SCOT open reading frame (Sino Biological Inc, Cat. HG15008-UT) for 48 h using Lipofectamine 2000 (Thermo Scientific) as per manufacturer's instructions. Culture media was collected and used for quantification of lactate levels using the Lactate Assay Kit II (Sigma-Aldrich, MO, USA).

Virtual High Throughput Screening

The SCOT (*Sus scrofa*) crystal structure was obtained from the Protein Data Bank (PDB: 1M3E) with a resolution of 2.5 Å (Bateman et al., 2002). The enzyme matched to *Homo sapiens*/*Mus musculus* SCOT with 92% similarity. The Sus scrofa SCOT structure was modified by adding the missing side chains and assigning the protonated groups at the neutral pH 7.0 (PROPKA 2.2). The protein was refined in terms of energy minimization and verified using PROCHECK, following which ready to dock commercially approved US Food and Drug Administration and investigational drugs (2924 ligands) were downloaded from the ZINC database. The CCSF CHIMERA v.1.10.2 was used to prepare the ligands for docking in the framework of AMBER99SB. VinaMPI was used to perform the blind docking by ''boxing'' the oxyanion pocket of the enzyme into a grid of 30 × 30 × 30 Å, with a spacing of 0.375Å. All rotatable bonds were allowed to rotate freely, and 20 runs were carried out for each ligand (Ellingson et al., 2013). After the initial run, all ligands were sorted based on their binding energies. The top 100 candidates were re-docked using the Autodock Vina with an exhaustiveness of 40. The final candidates were chosen based on their binding energy, binding interaction types, and ligand orientation in the oxyanion pocket. All visualizations were performed using the Discovery Studio Visualizer (Dassault Systèmes BIOVIA, 2015) and the Schrodinger's PyMOL package (Molecular Graphics System, Version 1.8).

Mutagenesis

The pCMV3 plasmid vector encoding wild-type SCOT was purchased from Sino Biologicals (PA USA). The mutants were generated using Quick Change Multi Site-Directed Mutagenesis Kit (Agilent Technologies, USA) by the manufacturer's instructions. The following two primers were used;

Ile323Ala Mutagenesis (Corresponds to* Sus scrofa *Ile284 in the crystal structure (PDB ID:1M3E))

(forward) 5′AGAAGAGGAATCCCAGCACCCAAGTTAGCGTACATGCCG3′

5′CGGCATGTACGCTAACTTGGGTGCTGGGATTCCTCTTCT3′ (reverse).

Lys368Ala Mutagenesis (Corresponds to* Sus scrofa *Lys329 in the crystal structure (PDB ID:1M3E))

(forward) 5′GAACAGTAACTGTTTCCGCTCCTGCATTGATGAGATCCGC3′

5′GCGGATCTCATCAATGCAGGAGCGGAAACAGTTACTGTTC3′(reverse).

All mutations were subsequently verified via DNA sequencing.

Succinyl-CoA:3-ketoacid-CoA Transferase Activity

C2C12 myotubes or gastrocnemius muscles were homogenized in PBS (pH 7.2) with protease inhibitors (complete mini EDTA-free protease inhibitor cocktail; Roche) in a glass dounce homogenizer on ice. Lysates were subsequently centrifuged at 20,000x g at 4°C for 20 min. The supernatants were then collected for the quantification of SCOT activity (μmol acetoacetyl-CoA produced/mg protein), which was measured spectrophotometrically by monitoring the absorbance changes at 313 nm at room temperature, and normalized to an acetoacetyl-CoA standard curve to determine rates of acetoacetyl-CoA production. The reaction mixture consisted of 50 mM Tris·HCl (pH 8.0), 10 mM $MgCl_2$, 0.2 mM succinyl-CoA, 0.1–10 mM lithium acetoacetate, and 4 mM iodoacetamide. The catalytic reaction was initiated by addition of 100 μg of protein from C2C12 myotube or gastrocnemius muscle lysates. The absorbance changes were recorded every 30 s from 0 to 3 min as previously described (Cotter et al., 2013).

In Vitro Kinetics Assessment

Recombinant human SCOT protein was purchased from MyBiosource (San Diego, CA, USA; MBS9420519). SCOT activity was measured by detecting acetoacetyl-CoA formation spectrophotometrically by monitoring the absorbance changes at 313 nm at room temperature. Activity of 0.45 nmol recombinant SCOT was measured on increasing acetoacetate concentrations (0.1, 0.5, 1, 2.5, 5 and 7.5 mM) in the presence of increasing pimozide concentrations (125 and 500 nM) using DMSO as a control. Data were presented as mean reaction rate (μmol/min) versus acetoacetate concentration and lines show fitting to the Michaelis–Menten equation with 95% confidence intervals. A Lineweaver–Burk plot data analysis from the Michaelis–Menten kinetics was used to determine the type of inhibition of SCOT by pimozide, and lines show fitting to linear regression with 95% confidence intervals.

Western Blotting

C2C12 myotubes or frozen skeletal muscle tissues (20 mg) were homogenized in buffer containing 50 mM Tris HCl (pH 8 at 4°C), 1 mM EDTA, 10% glycerol (w/v), 0.02% Brij-35 (w/v), 1 mM DTT, protease and phosphatase inhibitors (Sigma), and protein samples were prepared and subjected to western blotting protocols as previously described (Ussher et al., 2014). SCOT (ProteinTech, 12175-1-AP), acetyl-CoA acetyltransferase (ACAT) (Invitrogen, PA5-19227), heat shock protein-90 (Hsp90) (BD Biosciences, 610418), pan anti-succinyl lysine (PTM Biolabs, PTM-401), anti-cysteine sulfonate (Aviva Systems Biology, OAED00119), protein kinase B (Akt) and phospho-Akt (9272S and 4060L (Cell Signaling)), glycogen synthase kinase 3β (GSK3β) and phospho-GSK3β (5676S and 9331L (Cell Signaling)), pyruvate dehydrogenase (PDH) and phospho-PDH (3205S, Cell Signaling and ABS204, Millipore), 5′AMP activated protein kinase (AMPK) and phospho-AMPK (5831S and 2535S (Cell Signaling)), Na^+/K^+ ATPase (3010S (Cell Signaling)), and protein kinase Cθ (PKCθ) (13643S (Cell Signaling)) antibodies were prepared in a 1/1000 dilution in 5% BSA. Secondary antibodies consisted of anti-rabbit IgG (Cell Signaling, 7074V), anti-mouse IgG (Cell Signaling, 7076V), and anti-goat IgG (Thermo Fisher Scientific, A15963), all of which were prepared in a 1/2000 dilution in 1% fat-free milk. For the assessment of membrane PKCθ expression, membrane and cytosolic fractions were first prepared from frozen skeletal muscle tissues (~30 mg) using the Mem-PER Plus Membrane Protein Extraction Kit (Thermo Fisher Scientific, 89842), following which they were subjected to the above described western blotting protocols.

Real-Time Polymerase Chain Reaction Analysis

First-strand cDNA was synthesized from total RNA using the SuperScript III synthesis system (Invitrogen, Carlsbad, CA). Real-time PCR was carried out with the CFX connect Real time PCR machine (Bio-Rad Laboratories) using TaqMan Gene Expression Assays (Applied Biosystems, Foster City, CA) or custom designed SYBR Green primers (Kapa Biosystems) (Table S1). Relative mRNA transcript levels were quantified with the $2^{-\Delta\Delta Ct}$ method (Livak and Schmittgen, 2001) using peptidylprolyl isomerase A (*Ppia*) as our housekeeping internal control gene.

Determination of Triacylglycerol Content

Frozen powdered gastrocnemius or liver tissue (~20 mg) was extracted in a 2:1 chloroform:methanol solution, following which the supernatant phase was retained for the assessment of triacylglycerol (TAG) content with an enzymatic assay kit (Wako Pure

Chemical Industries) as previously described (Ussher et al., 2010). This same kit was also used to assess circulating TAG levels in mouse plasma samples (4 μL) as previously described (Ussher et al., 2010).

Determination of Diacylglycerol Content

Diacylglycerol (DAG) content was assessed in gastrocnemius muscle tissue (~20 mg) using a DAG fluorometric assay kit as per manufacturer's instructions (Abcam; Ab242293), which utilizes a kinase to yield phosphatidic acid, following which a lipase is utilized to hydrolyze phosphatidic acid to glycerol-3-phosphate. The glycerol-3-phosphate product is subsequently oxidized by glycerol-3-phoshate oxidase into a hydrogen peroxide that reacts with a fluorometric probe for quantitative measurement.

Determination of Glycogen Content

Glycogen content was assayed as previously described (Kim et al., 2017). In brief, glycogen was extracted from ~10-20 mg of powdered tissue with KOH and precipitated with sodium sulfate in ethanol for 1 h at −80°C. Glycogen was then pelleted and washed with ethanol. Amyloglucosidase was subsequently added and incubated at 55°C for 3 h. Glucose released from glycogen was measured by the glucose oxidase reaction. Samples were quantified against glycogen standards run in parallel and normalized to tissue wet weight.

Metabolomic Profiling

~50 mg of frozen powdered gastrocnemius tissue was subjected to a targeted quantitative metabolomics approach using a combination of direct injection mass spectrometry (DI-MS) with a reverse-phase liquid chromatography (LC)-MS/MS assay as previously described (Sung et al., 2017). The method used combines the derivatization and extraction of analytes, and the selective mass-spectrometric detection using multiple reaction monitoring (MRM) pairs. Isotope-labeled internal standards are used for metabolite quantification. All the samples were thawed on ice and were vortexed and centrifuged at 13,000x g. 10 μL of each sample was loaded and dried in a stream of N_2, following which 20 μL of a 5% solution of phenyl-isothiocyanate was added for derivatization. After incubation, samples were dried again using an evaporator. Extraction of the metabolites was then achieved by adding 300 μL methanol containing 5 mM ammonium acetate. The extracts were obtained by centrifugation, followed by a dilution step with kit MS running solvent. MS analysis was performed on an API4000 Qtrap tandem MS instrument (Applied Biosystems/MDS Analytical Technologies, Foster City, CA) equipped with a solvent delivery system. The samples were delivered to the mass spectrometer by a LC method followed by a direct injection (DI) method. Data analysis was performed and concentrations were calculated using Analyst software. The operator(s) were blinded to genotype/treatment during metabolomic profiling.

Standards (Sigma-Aldrich, ON, CAN) utilized for identification purposes include: acetylornithine, asymmetric dimethylarginine, carnosine, creatinine, levodopa, dopamine, histamine, methionine sulfoxide, cis-hydroxyproline, trans-hydroxyproline, phenylethylamine, putrescine, sarcosine, serotonin, spermidine, spermine, taurine, tyramine, alanine, arginine, asparagine, aspartic acid, citrulline, glutamine, glutamic acid, glycine, histidine, leucine, isoleucine, lysine, methionine, ornithine, phenylalanine, proline, serine, threonine, tryptophan, valine, 3-methylhistidine, betaine, trimethylamine N-oxide, choline, nitro-tyrosine, tyrosine, kynurenine, creatine, alpha-aminoadipic acid, lactic acid, beta-hydroxybutyric acid, alpha-ketoglutaric acid, citric acid, butyric acid, isobutyric acid, propionic acid, succinic acid, fumaric acid, pyruvic acid, hippuric acid, methylmalonic acid, homovanillic acid, indole-3-acetic acid, uric acid, L-carnitine inner salt, acetyl-L-carnitine hydrochloride, propionyl-L-carnitine, butyryl-L-carnitine, hexanoyl-L-carnitine, octanoyl-L-carnitine, decanoyl-L-carnitine, dodecanoyl-L-carnitine, tetradecanoyl-L-carnitine, hexadecanoyl-L-carnitine, octadecanoyl-L-carnitine, N-stearoyl-D-erythro-sphingosylphosphorylcholine, 1,2-dilinolenoyl-sn-glycero-3-phosphocholine, 1,2-Dioctadecanoyl-sn-glycero-3-phosphocholine, 1-oleoyl-2-hydroxy-sn-glycero-3-phosphocholine, glucose, N^1, N^{12}-diacetylspermine, 4-hydroxyhippuric acid and HPHPA.

Isotopically labeled internal standards (Cambridge Isotope Laboratories, MA, USA) utilized for absolute quantification include: D_2-ornithine, ^{15}N-histidine, D_3-creatinine, D_3-DOPA, D_4-dopamine, ^{13}C-tyrosine, ^{13}C-D_3-methionine, D_3-proline, D_4-serotonin, D_4-putrescine, D_3-sarcosine, $^{13}C_2$-taurine, D_4-tyramine, ^{15}N-alanine, $^{13}C_6$-arginine, ^{15}N-asparagine, D_3-aspartic acid, D_7-citrulline, D_3-glutamic acid, D_5-glutamine, $^{13}C_2$-glycine, ^{13}C-leucine, ^{15}N-phenylalanine, ^{13}C-serine, D_2-threonine, $^{15}N_2$-tryptophan, D_8-valine, D_9-TMAO, $^{15}N_2$-uric acid, D_8-spermine, D_8-spermidine, D_6-N^1, N^{12}-diacetylspermine, D_6-asymmetric dimethylarginine, D_3-creatinine, D_9-choline chloride, D_9-betaine hydrochloride, D_1-sodium L-lactate, D_4-sodium beta-hydroxybutyrate, ^{13}C-alpha-ketoglutaric acid, D_4-citric acid, ^{13}C-butyric acid, ^{13}C-propionic acid, D_4-succinic acid, $^{13}C_2$-D_2-fumaric acid, ^{13}C-pyruvic acid, D_2-hippuric acid, methyl-D_3-malonic acid, and D_2-indole-3-acetic acid.

Succinyl CoA & Malonyl CoA Content

To quantify short chain CoA content, ~15 mg of frozen powdered gastrocnemius tissue was homogenized in 6% perchloric acid, following which the homogenate was kept on ice for 10 min prior to centrifugation at 12,000x g for 5 min at 4°C, and analyzed via HPLC as previously described (Ussher et al., 2009b).

Succinate Assay

A colorimetric assay (Abcam; Ab204718) was used to measure succinate content in frozen gastrocnemius muscle samples as per manufacturer's recommendations.

Assessment of Reduced & Oxidized Glutathione

A fluorometric assay (Abcam, Ab138881) was used to measure the reduced and oxidized glutathione levels (GSH and GSSG) in gastrocnemius muscle and liver samples as per manufacturer's recommendations. In brief, tissue was lysed in 1% NP-40, diluted 10x in reaction buffer, and then fluorescence was measured 10-40 min after addition of dye as previously described (Saleme et al., 2019).

Intracellular ^{13}C-β-hydroxybutyrate Content

Differentiated C2C12 myotubes were incubated with 1.2 mM of ^{13}C-βOHB overnight prior to treatment with 10 μM pimozide for 24 h. Cells were then collected and metabolites were extracted by repeated (9x) freeze-thaw cycles in 600 μL of 90% methanol using liquid N_2 for freezing and ice for thawing and vigorous vortexing after every cycle. Metabolites were then dried using a vacuum centrifuge and dissolved in 100 μL of water, which was run on an Agilent HILIC-Z column with dimensions 2.1 × 50 mm at a flow rate of 0.5 mL/min. Solvent A consisted of water with 25 mM ammonium formate adjusted to pH 7.5, while Solvent B consisted of 25 mM ammonium formate (pH 7.5) in 90% acetonitrile/10% water. Solutions were run isocratically with 95% solvent B, 5% solvent A on an Agilent 1200 HPLC system interfaced to an Agilent 6220 Time-of-Flight LC/MS operating in negative ion electrospray mode.

QUANTIFICATION AND STATISTICAL ANALYSIS

All values are presented as means ± standard error of the mean (SEM). Two-tailed, unpaired Student's t tests were used to assess statistical significance between two groups. Multiple groups or treatments were compared using one-way analysis of variance (ANOVA) or a two-way ANOVA followed by a Bonferroni post hoc analysis, as appropriate to the design and/or data distribution. Differences were considered significant when $p < 0.05$. No data were considered outliers by testing or were arbitrarily excluded. The sample sizes (indicated throughout) were chosen to equal to 4 or more for *in vitro* studies and 5 or more mice per group for *in vivo* experiments, which our previous studies have consistently required in order to observe statistically significant differences between groups (Aburasayn et al., 2018; Al Batran et al., 2018; Ussher et al., 2010). GraphPad Prism 6 software was utilized for all data analysis.